CHALMERS
UNIVERSITY OF TECHNOLOGY

Evaluation and Comparison of Single-Phase and Three-Phase Full-Bridge Topologies for a 50 kW Fast Charger Station

Master of Science Thesis

NADIA HASSANZADEH

Department of Energy and Environment
CHALMERS UNIVERSITY OF TECHNOLOGY
Gothenburg, Sweden 2018

Master's thesis 2018:NN

Evaluation and Comparison of Single-Phase and Three-Phase Full-Bridge Topologies for a 50 kW Fast Charger Station

NADIA HASSANZADEH

CHALMERS
UNIVERSITY OF TECHNOLOGY

Department of Energy and Environment
Division of Electric Power Engineering
Chalmers University of Technology
Gothenburg, Sweden 2018

Evaluation and comparison of Single-Phase and Three-Phase
Full Bridge topologies for a 50 kW fast charger Station
NADIA HASSANZADEH

Supervisor: Saeid Haghbin, Department of Energy and Environment
Examiner: Torbjörn Thiringer, Department of Energy and Environment

Master's Thesis 2018:NN
Department of Department of Energy and Environment
Division of Electric Power Engineering
Chalmers University of Technology
SE-412 96 Gothenburg
Telephone +46 31 772 1000

Typeset in LaTeX
Printed by [Name of printing company]
Gothenburg, Sweden 2018

Evaluation and comparison of Single-Phase and Three-Phase
Full Bridge topologies for a 50 kW fast charger Station
NADIA HASSANZADEH
Department of Department of Energy and Environment
Division of Electric Power Engineering
Chalmers University of Technology

Abstract

In this work the design of a phase-shift full-bridge (PSFB) converter with MOSFET switches for a 50 kW fast charger station is developed. For the DC/DC stage two designs are presented based on the single-phase and three-phase full-bridge (FB) topologies. The converters are rated for 50 kW power at 420 VDC using 700 VDC while operating at a switching frequency of 25 kHz. The main contribution of this document is to analyze and compare the efficiency of the single-phase and three-phase topologies.

For the PSFB converter, the control is performed by a fixed duty cycle slightly less than 50% for each leg. The phase-shift between the two legs determines the power transfer from the input supply to the load. Silicon Carbide (SiC) MOSFETs are utilized as the power switches, to ensure low switching losses of high switching frequencies. A nanocrystalline magnetic material is used for the transformer in order to have high flux densities and low losses. The ZVS range for the single-phase and three-phase converters are evaluated and it is found that the three-phase converter achieves ZVS throughout the operation range.

It has been shown that the overall efficiency of the single-phase converter for 25 kHz is above 99 percent at full load condition. The different losses in the converters are discussed. It is shown that the transformer loss is the dominant loss in those converters. *LCC* analysis of the two topologies based on the cost of components has been conducted, which shows that the single-phase converter is more cost efficient compared to the three-phase version. Design equations are derived to help with a suitable selection of components for a given specification. The system simulation has been done using MATLAB/PLECS software. The theoretical calculations have been verified with simulations. Some comparison results are described at the end of this work.

Keywords: DC/DC converter; full-bridge; ZVS; phase-shift; fast charger.

Acknowledgements

This work has been carried out at the Department of Energy and Environment at Chalmers University of Technology.
First, I would like to express my deep gratitude and appreciation to my supervisor, Dr. Saeid Haghbin and my examiner, Prof.Torbjörn Thiringer, for their time, knowledge and help during the thesis work.
I am especially indebted to Farzad Yazdani, Phd student in Sharif university in Iran and researcher at Chalmers. His great helps made my thesis work at Chalmers University possible.
My especial gratitude goes to Dr. Carl-Evert Olsson, for his support and patience. His broad vision on the technical issues and life are most valuable during my years of study in Chalmers.
My deepest gratitude belongs to my parents, my brother and my sister for their love, care and unconditional support for my study.

Nadia Hassanzadeh
Gothenburg, Sweden
May, 2018

Contents

1 Introduction **1**
- 1.1 Background . . . 1
- 1.2 Aim . . . 2
- 1.3 Sustainable Aspect . . . 2
- 1.4 Ethical Aspect . . . 2
- 1.5 Scope . . . 2
- 1.6 Limitations . . . 3

2 Theory **5**
- 2.1 Topology Review for High Power DC/DC Converter . . . 5
- 2.2 Switching Loss, Conduction Loss . . . 5
- 2.3 Transformer . . . 6
  - 2.3.1 Single-Phase Transformers . . . 6
  - 2.3.2 Three-Phase Transformers . . . 6
  - 2.3.3 Zero Sequence Impedance . . . 7
  - 2.3.4 Transformer Losses . . . 9
    - 2.3.4.1 The Coil Loss . . . 9
    - 2.3.4.2 The Core Loss . . . 9
  - 2.3.5 Transformer Design Consideration . . . 10

3 Methods **11**
- 3.1 Transformer Isolated Phase-Shifted Full-Bridge Converter . . . 11
  - 3.1.1 Principle of Operation . . . 11
    - 3.1.1.1 Initial Condition $t < t_0$ . . . 13
    - 3.1.1.2 The Right Leg Transition $t_0 < t < t_2$ . . . 13
    - 3.1.1.3 The Left Leg Transition $t_2 < t < t_3$ . . . 13
    - 3.1.1.4 The Power Transfer Interval $t_3 < t < t_4$ . . . 13
  - 3.1.2 Design of a Phase-Shift Full-Bridge DC/DC Converter . . . 15
    - 3.1.2.1 Resonance Circuit Calculation . . . 15
    - 3.1.2.2 Output Filter Design . . . 16
    - 3.1.2.3 Transformer Current Calculations . . . 16
    - 3.1.2.4 Output Diodes Current . . . 18
    - 3.1.2.5 The Mosfet Switch RMS Current . . . 19
  - 3.1.3 Zero Voltage Switching Range . . . 20
  - 3.1.4 Transformer Design Parameters for Single-phase DC/DC Converter . . . 21

3.1.4.1 Number of Turns in the Primary and Secondary Windings . . . 21
3.1.4.2 The Size of a Conductor . . . 21
3.1.4.3 The Resistance of the Primary and Secondary Winding 23
3.1.5 Power-Loss Analysis for the Phase-Shift Full-Bridge DC/DC Converter . . . 23
3.1.5.1 Switching Losses . . . 23
3.1.5.2 Conduction Losses . . . 23
3.1.5.3 Copper Losses . . . 24
3.1.5.4 Core Losses . . . 24
3.1.5.5 Total Losses and Efficiency . . . 24
3.2 A Three-Phase Full-Bridge DC/DC Converter with High-Frequency Isolation . . . 25
3.2.1 Analysis of the Three-Phase DC/DC Converter . . . 26
3.2.1.1 Three-Phase Converter Waveforms . . . 26
3.2.1.2 Principles of Operation . . . 28
3.2.1.3 The Input/Output Voltage Relation . . . 31
3.2.2 Phase Current Waveforms . . . 32
3.2.2.1 RMS Current of Components . . . 33
3.2.2.2 Average Current of Components . . . 34
3.2.3 Mosfet Switches Behavior During Turn on and off . . . 35
3.2.3.1 Turn on the Switch . . . 35
3.2.3.2 Turn off the Switch . . . 36
3.2.4 Transformer Design Parameters for Three-Phase DC/DC Converter . . . 37
3.2.5 Evaluation of Different Losses in the Three-Phase Converter . 38
3.2.5.1 Switching Losses . . . 38
3.2.5.2 Conduction Losses of the Mosfet Switch . . . 38
3.2.5.3 Conduction Losses of the Body Diode of the Switch . 38
3.2.5.4 Conduction Losses of the Rectifier Diode . . . 39
3.2.5.5 Copper Losses of the Transformer . . . 39
3.2.5.6 Core Losses of the Transformer . . . 39
3.2.5.7 Total Losses and Efficiency . . . 40

4 Results **41**
4.1 The Design of a 50 kW Single-Phase Phase-Shifted Full-Bridge Converter . . . 41
4.1.1 Transformer Selection . . . 41
4.1.2 Switch Selection . . . 42
4.1.3 Output Rectifier Diode Selection . . . 42
4.1.4 Converter Design Calculation . . . 42
4.1.5 Zero Voltage Switching Range . . . 44
4.1.6 Transformer Parameters Calculation for Single-Phase DC/DC Converter . . . 46
4.1.6.1 Primary Winding Calculation . . . 46
4.1.6.2 Secondary Winding Calculation . . . 47

4.1.7 Total Loss Calculation for Single-Phase DC/DC Converter . . 48
4.1.8 Total Losses of Single-Phase DC/DC Converter 49
4.1.9 Efficiency of Single-Phase DC/DC Converter 51
4.2 The Design of a 50 kW Three-Phase Full-Bridge DC/DC Converter . 52
4.2.1 Design of the Leakage Inductance (L_a) 52
4.2.2 Design of the Magnetization Inductance (L_m) 52
4.2.3 Design of the Output Filter Inductance 53
4.2.4 Design of the Output Capacitance 53
4.2.5 Transformer Selection 53
4.2.6 Transformer Parameters Calculation for Three-Phase DC/DC Converter 54
4.2.6.1 The Number of Turns in the Primary and Secondary Winding of the Transformer 54
4.2.6.2 Resistance of the Primary Winding 54
4.2.6.3 Resistance of the Secondary Winding 55
4.2.7 Total Loss Calculation for Three-Phase DC/DC Converter . . 56
4.2.8 Total Losses of Three-Phase DC/DC Converter 57
4.2.9 Efficiency of Three-Phase DC/DC Converter 59
4.3 Life Cycle Cost Analysis ($LCCA$) 60
4.3.1 Development of $LCCA$ Model 60
4.3.1.1 Project Cost 60
4.3.1.2 Net Present Value 60
4.3.2 LCC Model Analysis for $PSFB$ Converter 61
4.3.2.1 Project Cost 61
4.3.2.2 Energy Cost 63
4.3.2.3 LCC Analysis 64
4.3.2.4 Pareto Plot 65
4.4 Comparison Between Single-Phase and Three-Phase DC/DC Converter 66
4.5 Results of the Simulation 68
4.5.1 The Simulation of the Single-Phase Converter 68
4.5.2 The Simulation of the Three-Phase Converter 70

5 Conclusion and Future Work **73**
5.1 Results From Present Work 73
5.2 Future Work 74

Bibliography **75**

A Appendix 1 **I**
A.1 Paper I

1
Introduction

1.1 Background

One of the most critical issues regarding local pollution is reducing the pollution generated by hydrocarbon combustion of transportation vehicles. In the light of this, hybrid electric vehicles (HEV) and full electric vehicles (EV) are providing a solution through the use of a battery pack, which supplies energy for the electric system. One of the frequently used topologies for a charger station is an AC/DC conversion followed by an isolated DC/DC stage. DC/DC converters provide proper voltage levels and the power management between different energy sources and storage elements. The topology is based on two switching converters, linked through a high frequency transformer, which provides the galvanic isolation between the high voltage side and low voltage side for safety reasons.

Although the battery capacity of the electric vehicles (EVs) is sufficient for short trips, the needed time for charging is one of the challenges for EVs as an alternative to internal combustion engines (ICE). The other problem with currently available DC fast chargers is the low-frequency switching which increases the size, weight, and cost of these fast chargers. Nowadays, there are some experiments of fast chargers for the urban electrical buses like electrical buses in Santa Barbara, in U.S., and electrical buses recently presented in Geneva, Switzerland and Sweden [1]. The trends is towards a smaller size and more efficient stations while the cost is reduced [2].

In order to demonstrate a practical example of an electric charging system, several studies have been done. For instance in [3], an automatic fast charger station with a power level of 120 kW is developed for city Bus Line 60 in Gothenburg, Sweden based on a hybrid electric bus. In this work, in order to eliminate low order current harmonics and to obtain a unity power factor operation, it is suggested to replace the passive diode rectifier with an active front-end converter. In [4] the current status and implementation of battery chargers, charging power levels, and infrastructure for plug-in electric vehicles and hybrids have been discussed. It has been shown that, the major issues are the battery prices and required charging infrastructures for a common utilization of PHEBs.

Furthermore, the recent improvement in the materials and tools enhance the overall power density in charger systems. The idea is to reduce the components size, by increasing the switching frequency. In [5] two different designs based on a single-phase Full-bridge and a Dual Active Bridge topology for the DC/ DC stage of a

50 kW charger has been proposed. The suggested designs in [5] improve the power density by applying high-frequency switching. The recent research is paving the way for a fair comparison of other topologies, which has been discussed in this work.

1.2 Aim

The aim of this project is to evaluate and compare two different topologies, single-phase full bridge and three-phase full bridge for the DC/DC stage of a 50 kW fast charger station with respect to the efficiency, and the total converters costs.

1.3 Sustainable Aspect

Nowadays in industrialized countries, there is a high interest to produce hybrid electric vehicles (HEV) and full electric vehicles (EV) by the governments and public. The three principal concepts of sustainable development are "Social justice", "Environmental protection", and "Economic development". From eco-environmental perspective, EVs can be considered as a sustainable means of transportation when the electricity for charging the batteries for the EVs is generated by renewable energies such as hydroelectric power, hybrid solar photovoltaic, wind power and nuclear fusion.
In term of sustainability of EVs related to the batteries, the energy required to produce batteries, emissions and environmental impact in recycled consumed batteries must be considered [6].

1.4 Ethical Aspect

The power electronic components must be designed in a secure way to mitigate the health risk in accordance with the IEEE code of ethics, #1: "to accept responsibility in making decisions consistent with the safety, health, and welfare of the public, and to disclose promptly factors that might endanger the public or the environment" [7]. The DC/DC converter with all power electronic components will be isolated with a non-conductive enclosure to ensure that there will be no threat to the user. As another protective measure, current limiting fuses will be considered in order to protect against a short circuit failure.

1.5 Scope

In this project, design and simulation with Matlab/Simulink for a 50 kW DC/DC converter based on a single-phase and three-phase full bridge topology are discussed. For the 50 kW fast charger station, a full bridge topology with isolated transformer-soft switched for high power density is a suitable choose.

1.6 Limitations

In this work some limitations have been considered.

- The DAB set-up has not been discussed.
- For the design of a three phase transformer one common three phase core is presently not available, due to the the manufacturing technology. In this work instead a design of a three phase transformer, 3 single core have been considered.
- The price of the DC-link capacitor has not been considered.

2

Theory

2.1 Topology Review for High Power DC/DC Converter

The dc/dc converter is an important component in a power charger application. The first step in designing an isolated dc-dc power converter, is the selection of the topology. Mainly, a topology selection is based upon the desired output power level, battery voltage, the efficiency of the converter, initial cost and long term operation expense. One of the topologies, which is used in high input voltage and high-power applications, is the phase-shifted full-bridge converter. The phase-shifted full-bridge converter (PSFB) operates in zero-voltage switching of the primary switches while keeping the switching frequency constant. By using a leakage inductor in series with the primary side of the power transformer, zero-voltage switching is achieved. However at light-load conditions, ZVS may be lost which will be discussed in detail in the following sections [8].

In order to have high power densities of a converter, operation at higher switching frequencies is required, which reduces the size of transformers and filters. However, by increasing switching frequencies, the switching losses related to the turn-on and turn-off of the switches also increases. Thanks to the zero voltage or zero current switching topologies, which reduces the switching losses, operation of the converter at high frequency switching is achievable. Therefore, the Phase-Shifted Full Bridge DC/DC converter with ZVS operation at high switching frequency has higher efficiency, higher power density, with lower size and cost.

2.2 Switching Loss, Conduction Loss

The main power losses in a DC/DC converter are switching losses and conduction losses of switches and diodes. The switching losses are related to the overlap of voltage and current waveforms during switches turn-on and turn-off, which are dependent on the voltage applied over the switch, and the current flowing through the switch. The conduction losses are based on switches resistive losses and diodes voltage drop losses. The switch resistive loss can be calculated by the resistance of the switch multiplied with the second order of the RMS value of the switch current. The diode conduction losses are obtained by the turn-on voltage of the diode, and

the averaged value of the diode's current.

In high voltage and high-power applications, the switching losses dominate, due to the high input voltage applied over the switches. By using the soft-switching, which removes switching losses, it gets help to improve system efficiency [9]. In order to decrease conduction losses, a metal-oxide-semiconductor-field-effect-transistor (MOSFET) based on Silicon Carbide (SiC) should be used, which reduce conduction losses due to the low on resistance in comparison with similar devices [5]. Furthermore, choosing low forward voltage drop diodes for the output rectifier helps to reduce conduction losses.

2.3 Transformer

2.3.1 Single-Phase Transformers

A single-phase transformer consists of two electrically isolated windings, wound around two legs of a magnetic core, one on the primary side connected to the electrical power source, and the other on the secondary side connected to a load . They are mostly used in single-phase circuit. The core of transformer is either square or rectangular type, which is divided into two parts vertical and horizontal. The vertical part on which coils are wound called limb, while horizontal part is called yoke [10], [11].

2.3.2 Three-Phase Transformers

A three-phase transformer with three windings wound on a three-legs magnetic core is usually used in a three-phase circuit. A primary and a secondary winding are placed one on top of the other on each of the three legs of the core. A core-type transformer can have three, four or five legs. A bank of three single-phase transformers also can be used in a three-phase circuit. The three-phase transformer with a common core is a cheaper one with smaller size and less weight. The main disadvantage of the three-phase transformer with a common core is that if one phase becomes defective, then the whole transformer needs to be replaced. The advantages of three single-phase units are transportation, maintenance and spare unit availability. In a three-legged core-type transformer the magnetic flux of one phase is returned through the other two phases. During ordinary operation the total magnetic flux is expected to be zero [10], [11].

2.3.3 Zero Sequence Impedance

When a three-phase transformer is subjected to abnormal supply voltages and unbalanced loadings, the positive and negative sequence impedance values are identical to symmetrical components, but the zero-sequence impedance of a three-phase transformer depends on the type of winding connections on each side, and the core construction. Its equivalent circuit depends on the path available for the flow of zero-sequence flux within the transformer magnetic circuit [10].

As in a three-legged transformer there is no physical low magnetic-reluctance path from top to the bottom of the core, then the zero-sequence flux must go from the top yoke through the air gap, into the tank. As the air gap has high magnetic reluctance then, the magnetic impedance of the zero-sequence flux, which is inversely proportional to the magnetic reluctance, is very low. Under unbalanced condition, the zero-sequence current will be large, and the core and tank may have unacceptable temperature [10].

In order to provide lower magnetic reluctance for the zero-sequence flux, mainly close to the positive-sequence magnetic reluctance, a fourth or fifth leg is added to the transformer core structure, which provides a magnetic low-reluctance return path for the zero-sequence flux in the transformer. The additional leg in the four-leg transformer is designed to have the same size of the other legs. The five-leg transformer has two additional legs with almost half size as compared to the main legs. The zero-sequence returned flux in a four or five-leg transformer is respectively, 3 or 1.5 times the flux flowing at each leg surrounded by the winding. In a four or five-leg transformer when the zero-sequence voltage approaches a certain value of the rated voltage the additional legs begin to saturate, and the magnetic impedance begins to drop [10], [12]. Schematics of three-legged, four and five-legged core-type transformer magnetic paths are shown in Fig. 2.1.

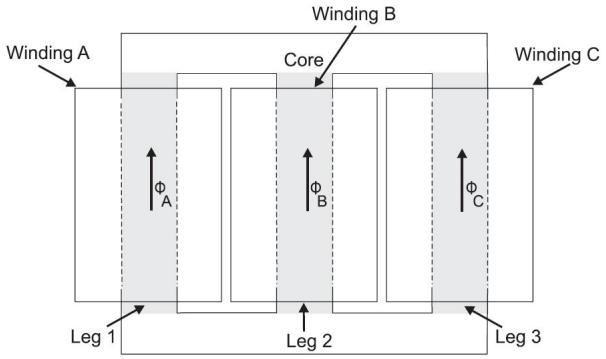

(a)

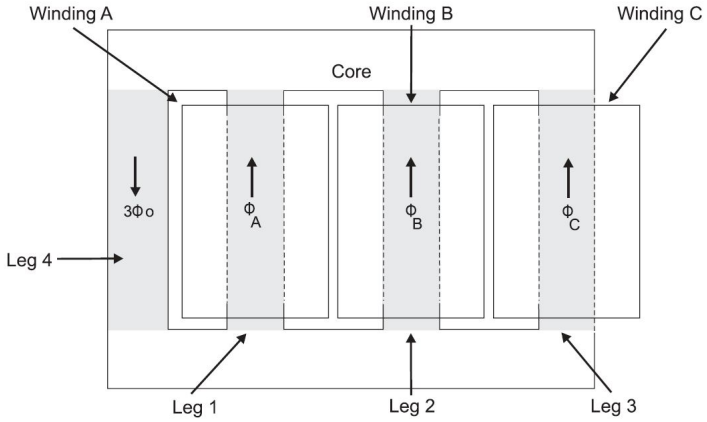

(b)

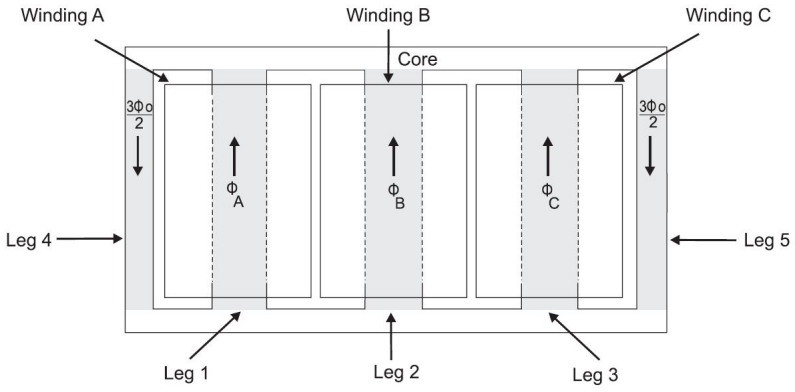

(c)

Figure 2.1: Schematic of core-type transformer magnetic paths (a) three-legged (b) four-legged (c) five-legged

2.3.4 Transformer Losses

The total transformer losses are a sum of coil and core losses, which are produced by the electrical current flowing in the coils and the alternating flux in the core of the transformer. The losses related with the coils are called the load losses, which vary with the transformer loading. The losses produced in the core are called no-load losses, these losses occur in the transformer core whenever the transformer is energized (even when the secondary circuit is open), and do not vary with the loading on the transformer [13].

2.3.4.1 The Coil Loss

Ohmic heat losses, or RI^2 losses, in the winding conductors are the main part of the load losses. The magnitude of heat losses increases with the square of the load current and is proportional to the resistance of the winding. By increasing the cross-sectional area of the conductor or by reducing the winding length, the resistance of the conductor decreases which results to reduce the losses [13].

2.3.4.2 The Core Loss

The core loss is the sum of three components: *hysteresis loss, eddy current loss and the excess loss* [13].

- Hysteresis Loss
Hysteresis losses come from the molecules in the core resisting being magnetized and demagnetized by the alternating magnetic field. This resistance by the molecules causes friction that result in heat. These losses depend on the type of material used to build a core. By changing the size and type of core material, hysteresis losses can be reduced.

- Eddy-Current Loss
By Faradays law, the change in flux through the core induces circulating currents in the core and are responsible for resistive heating of the core. Eddy current losses can be minimized by reducing the thickness of lamination and increasing the resistivity of the material in the core.

- Excess Loss
Due to the presence of leakage field, there are excess losses in the material. The percentage of these losses are very small as compared to the hysteresis and eddy losses so they can be neglected.

- Core Loss Calculation

To calculate the core loss, Steinmetz proposed an empirical equation

$$P_{core} = k f^{\alpha} B^{\beta} \tag{2.1}$$

which is widely used nowadays.It's simple, but only valid for sinusoidal excitation. So, **an improved general Steinmetz equation** is proposed for arbitrary waveform. According to the **IGSE** the transformer core loss per unit volume is expressed as [14],

$$P_v = \frac{K_i}{T} \int_0^T |\frac{dB}{dt}|^{\alpha} |\Delta B|^{\beta-\alpha} dt \tag{2.2}$$

and the transformer core loss is given by

$$P_{Core} = P_v V_e \tag{2.3}$$

where f is the fundamental frequency of the excitation, and B is the maximum flux density, K_i, α and β are the core material constants, and can be easily obtained by manufacturer datasheets, and V_e is the total volume of the core [14].

2.3.5 Transformer Design Consideration

Design changes to reduce transformer losses, always involve trade offs. For example, consider varying the cross-sectional area of the transformer core. An increase tends to lower no-load loss while raising the winding loss. An increase in volts per turn reduces winding loss while increasing the core loss.

Unfortunately, some efforts to reduce winding losses increase core losses and vice versa. For example, increasing the amount of conductor used reduces the winding losses, but it may necessitate using a larger core, which would increase core losses. Manufacturers are developing techniques that optimize these losses based on the expected loading [13].

3

Methods

3.1 Transformer Isolated Phase-Shifted Full-Bridge Converter

An isolated DC/DC converter is followed by a front-end AC/DC converter in the battery charger circuit. The role of the AC/DC converter is power factor correction which is out of the scope of this work. The isolated phase-shifted full-bridge converter operates under zero voltage switching by utilizing the advantage of the transformer leakage inductance and the junction capacitance of the power transistor to achieve resonant switching with no additional snubbers. The significant advantage of the isolated phase-shifted full-bridge converter compared to the conventional full bridge converter is its high efficiency due to the reduction of switching losses which is the result of ZVS operation. The ZVS enables high switching frequency operation with high power density and conversion efficiency [15], [16]. Here the effect of the phase–shift operation of switches and the resonance between the transformer leakage inductance and the capacitance of the power transistor will be discussed.

3.1.1 Principle of Operation

The phase-shifted full-bridge DC/DC converter with zero voltage switching operation is shown in Fig. 3.1. There are two legs in the bridge with four power transistor switches, considered constant duty cycle around 50% for each leg in order to control the output voltage. The gate signals turn on/off the switches in the bridge with a phase shift between the duty cycles of any two diagonally switches in the left leg and the right leg. This phase shift between the two legs determines the duty cycle of the converter and enforces how much power transfer that takes place from the input supply to the charger. With a phase shift of zero, the duty cycle will be 1 which results in hard-switched operation of the converter. In the case that the phase-shift angle equals 180 degrees, the duty cycle will be zero and there is no power transfer. The gate signals, the primary current, the voltage in the primary and secondary of the transformer are presented in Fig. 3.2. The switching period T_s and the duty cycle D are shown in the figure too.

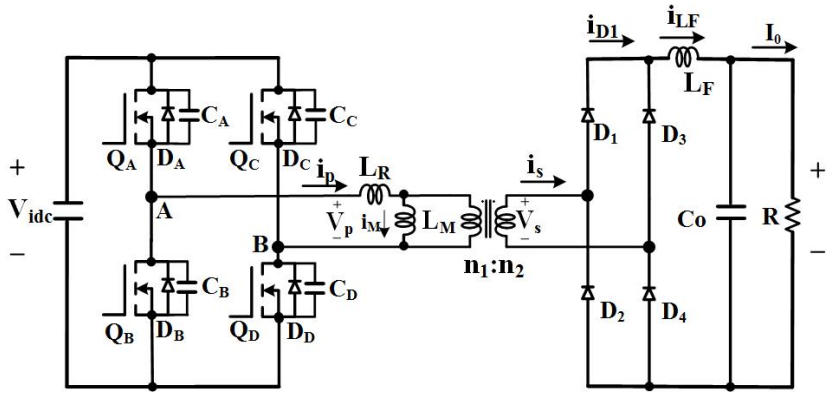

Figure 3.1: Phase-shifted full-bridge converter with ZVS operation

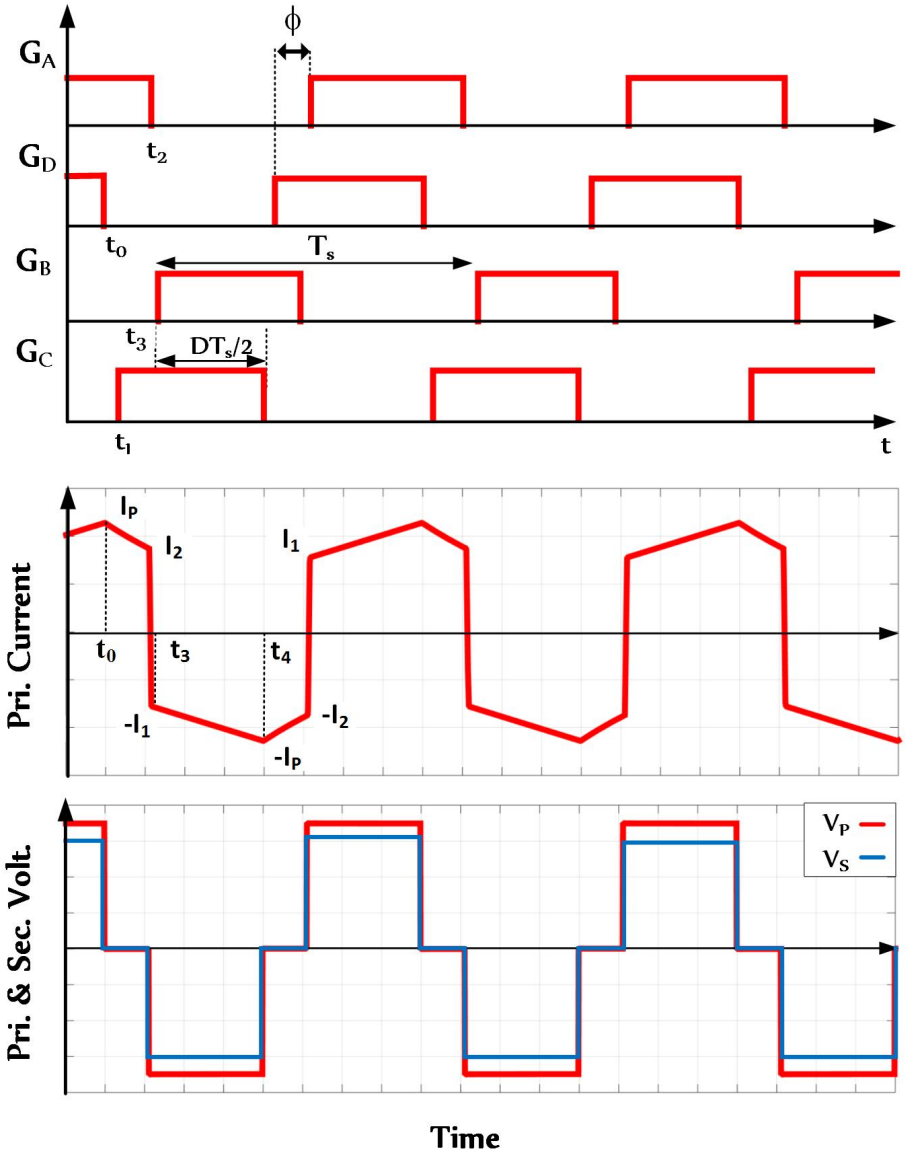

Figure 3.2: The waveforms of the phase-shifted full-bridge converter

3.1.1.1 Initial Condition $t < t_0$

Switches Q_A and Q_D are conducting and on the secondary side of the converter the diodes D_1 and D_4 are conducting current through the output inductor L_F to the output load of the converter. The zero voltage switching will be obtained by using the energy stored in the leakage inductance of the transformer to discharge the output capacitor of the switches in order to get zero voltage across the switches before turning on.

3.1.1.2 The Right Leg Transition $t_0 < t < t_2$

At time t_0, the right leg transition initiates by turning off Q_D. The current through the primary of the transformer charges the output capacitor of Q_D and discharges the output capacitor of Q_C. Subsequently, after fully discharging C_C, the input diode of switch Q_C conducts the current. If the switch Q_C turns on the voltage across the switch is zero. At time t_0, when the switch Q_D turns off, the primary current of the transformer is in the peak value which is the reflected current of the secondary of the transformer with a large current of the output filter. Then ZVS can be achieved for Q_C and Q_D easily even at the light loads. In the right leg transition, after discharging C_C , the current circulates between D_C and the transistor Q_A, then the transformer primary voltage decreases and at the end of this time interval the primary voltage is zero. On the secondary side also the secondary voltage of transformer goes to zero and after that the output filter supplies the load current.

3.1.1.3 The Left Leg Transition $t_2 < t < t_3$

At time t_2, the left leg transition starts by turning off Q_A. For switches Q_A and Q_B the ZVS mechanism is different. The ZVS is provided by the resonance between the leakage inductance of the transformer and the output capacitance of the switches. In the secondary side of the converter all diodes are conducting and there is a short circuit across the secondary side of the transformer. Then the primary current of the transformer is $i(t_2)$ which is less than the peak value. The stored energy in the leakage inductance has to be larger than the stored energy in the output capacitor of the switch in order to get ZVS. In this case for the light loads, the ZVS will be lost. With high input voltage which requires more capacitive energy, the condition gets worse.

3.1.1.4 The Power Transfer Interval $t_3 < t < t_4$

After discharging capacitor C_B, the internal diode of the switch conducts the current. If the switch Q_B turns on at t_3, the left leg transition will be completed. After this time interval, the voltage in the primary of the transformer is V_i. At time t_4 the switch Q_C turns off, and it provides the leakage inductor's current to flow through switch Q_B and the output capacitances of Q_C and Q_D. Then the process continues as before. The circuit diagram at each time intervals is shown in Fig. 3.3.

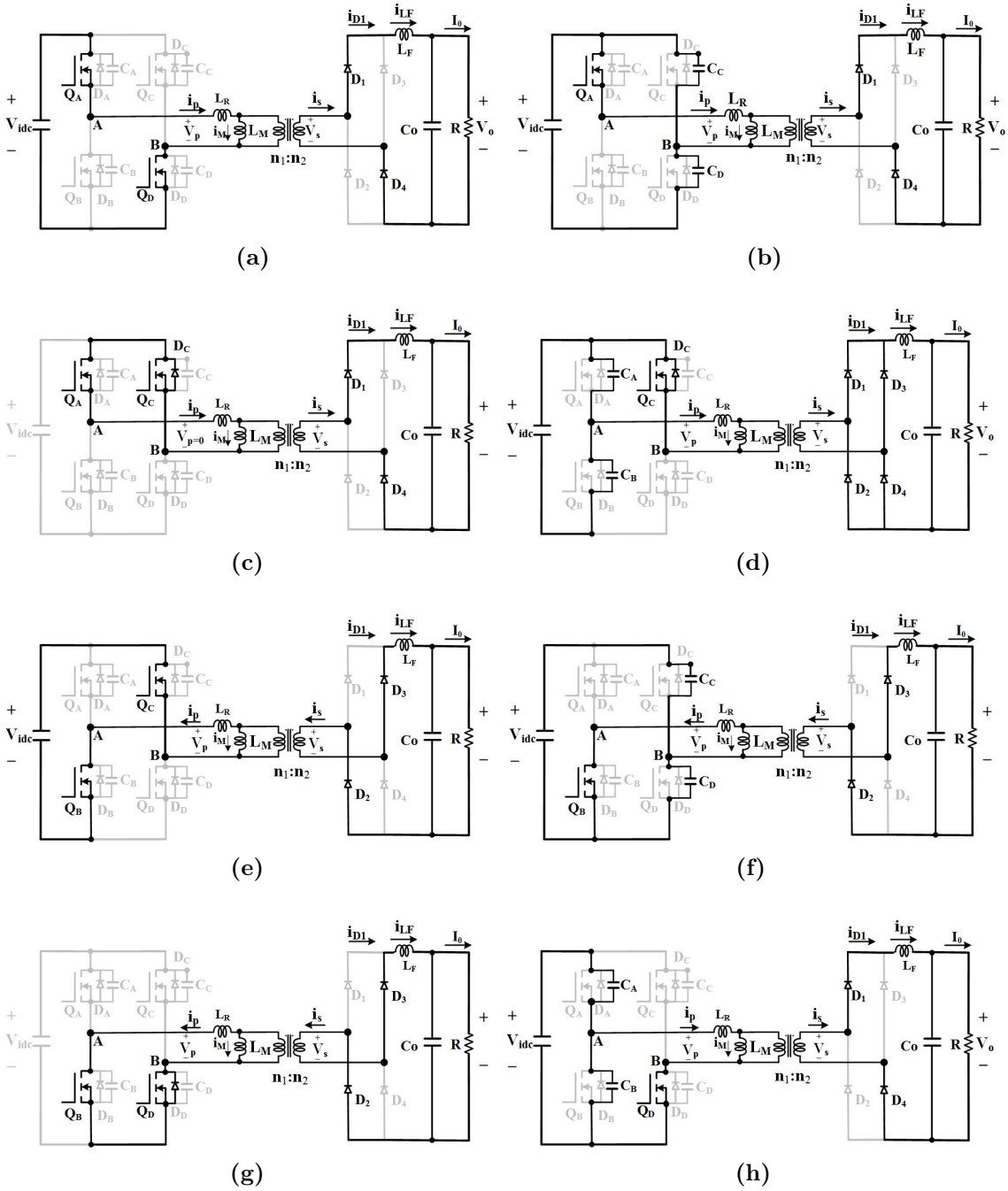

Figure 3.3: Operation of the Phase-Shifted Full-Bridge Converter
(a) Initial condition $t < t_0$ (b) The right leg transition $t_o < t < t_1$
(c) The right leg transition $t_1 < t < t_2$ (d) The left leg transition $t_2 < t < t_3$
(e) The power transfer interval $t_3 < t < t_4$ (f) The right leg transition $t_4 < t < t_5$
(g) The right leg transition $t_5 < t < t_6$ (h) The left leg transition $t_6 < t < t_7$

3.1.2 Design of a Phase-Shift Full-Bridge DC/DC Converter

This section defines the design procedure and component selection for a 50 kW PSFB converter. The first step in the design would be determining D_{max} which determines the maximum turns-ratio of the transformator. The maximum and minimum duty cycle is defined as [15]

$$D_{min} = \frac{nV_{o,min}}{V_{idc}} \tag{3.1}$$

$$D_{max} = \frac{nV_{o,max}}{V_{idc}} \tag{3.2}$$

where $V_{o,min}$ and $V_{o,max}$ are the minimum and maximum output voltage, V_{idc} is the input voltage. The transformer turns-ratio (n) is the number of the turns of the winding in the primary over the secondary.

3.1.2.1 Resonance Circuit Calculation

The achievement of the high efficiency of power conversion needs to ensure ZVS operation at the light-load condition, since the output power depends on the leakage inductance of the transformer and the switching frequency at low load [17]. By increasing the leakage inductance, ZVS operation will be obtained in a wide range, but this results in a duty cycle loss in the secondary side, and circulating current in the rectifier [18]. For achieving ZVS operation, the energy stored in the leakage inductance must be more than the energy needed for charging and discharging the output capacitance of the switches during a dead time [16]. The required energy in the resonance inductance L_R is as below

$$E = \frac{1}{2}L_R I_2^2 > \frac{4}{3}C_{oss}V_{idc}^2 + \frac{1}{2}C_T V_{idc}^2 \tag{3.3}$$

where L_R is the transformer leakage inductance, C_{oss} is the switch output capacitance, C_T is the transformer winding capacitance, I_2 is the primary current of the transformer at t_2 or t_6 and V_{idc} is the input voltage. The factor of $\frac{4}{3}C_{oss}V_{idc}^2$ is the estimation of two times the stored energy in the switches output capacitance in the resonance circuit. In order to find the proper resonant inductance 50% of the full load is considered for calculation [15]. The equivalent resonant capacitance can be calculated as

$$C_R = \frac{8}{3}C_{oss} + C_T. \tag{3.4}$$

3.1.2.2 Output Filter Design

The output inductor, L_f , can be calculated as [15]

$$L_f = \frac{V_{o,nom}(1 - D_{nom})}{4\triangle I_o f_s} \tag{3.5}$$

where $V_{o,nom}$ is the output voltage, $D_{nom}$is the nominal duty cycle, f_s switching frequency, and $\triangle I_o$ is the output current ripple.

The output capacitor is expressed by considering the time during the load transient, then the output capacitor is calculated as [15]

$$C_o \geq \frac{\triangle I_o T_s}{16\triangle V_o}. \tag{3.6}$$

3.1.2.3 Transformer Current Calculations

In order to control the converter under peak current mode, the peak value of the output inductor current should be more than the magnetization current, that means $I_M \leq \triangle I_o/n$. Then the magnetization inductance of the transformer can be calculated as [15]

$$L_M \geq \frac{nDV_{idc}}{4\triangle I_o f_s}. \tag{3.7}$$

Then the magnetization current can be expressed as

$$I_M = \frac{DV_{idc}}{4L_M f_s}. \tag{3.8}$$

The transformer primary current is shown in Fig. 3.4. There are three significant current levels in the transformer primary current which are defined as [15]

$$I_P = I_M + \frac{I_o + \triangle I_o}{n} \tag{3.9}$$

$$I_1 = -I_M + \frac{I_o - \triangle I_o}{n} \tag{3.10}$$

$$I_2 = I_M + \frac{I_o - \triangle I_o}{n}. \tag{3.11}$$

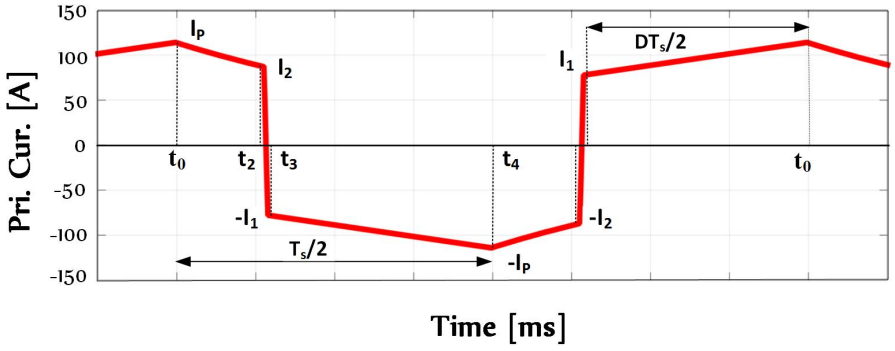

Figure 3.4: The transformer primary current

With some mathematical manipulation, one can calculate the RMS value of the primary current of the transformer as below [15]

$$\begin{aligned} I_{P,rms}^2 = &\frac{1}{3}(-I_P + I_2)^2 D_1 + (-I_P + I_2) I_P D_1 + I_P^2 D_1 \\ &+\frac{1}{3}(-I_2 - I_1)^2 D_2 + (-I_2 - I_1) I_2 D_2 + I_2^2 D_2 \\ &+\frac{1}{3}(-I_P + I_1)^2 D + (-I_P + I_1)(-I_1) D + I_1^2 D. \end{aligned} \tag{3.12}$$

The parameters D, D_1 and D_2 can be written as [15]

$$D + D_1 + D_2 = 1 \tag{3.13}$$

$$D = \frac{t_4 - t_3}{T_s/2} \tag{3.14}$$

$$D_1 = \frac{t_2}{T_s/2} \tag{3.15}$$

$$D_2 = \frac{t_3 - t_2}{T_s/2}. \tag{3.16}$$

From Fig. 3.4 it can be seen that $t_3 - t_2$ related to the right leg transition that can be calculated as

$$t_3 - t_2 = \frac{1}{4} T_R = \frac{1}{2} \frac{\pi}{\omega_R}. \tag{3.17}$$

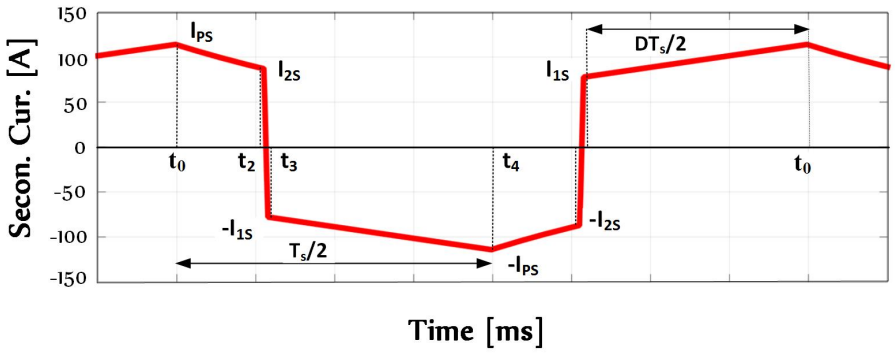

Figure 3.5: The transformer secondary current

The transformer secondary current is depicted in Fig. 3.5. Here also there are three important current levels as describe below [15]

$$I_{Ps} = I_o + \triangle I_o \tag{3.18}$$

$$I_{1s} = I_o - \triangle I_o \tag{3.19}$$

$$I_{2s} = I_o - \triangle I_o - nI_M. \tag{3.20}$$

The RMS value of the secondary side of the transformer can be calculated as [15]

$$\begin{aligned} I_{S,rms}^2 = &\frac{1}{3}(-I_{PS} + I_{2S})^2 D_1 + (-I_{PS} + I_{2S}) I_{PS} D_1 + I_{PS}^2 D_1 \\ &+\frac{1}{3}(-I_{2S} - I_{1S})^2 D_2 + (-I_{2S} - I_{1S}) I_{2S} D_2 + I_{2S}^2 D_2 \\ &+\frac{1}{3}(-I_{PS} + I_{1S})^2 D + (-I_{PS} + I_{1S})(-I_{1S}) D + I_{1S}^2 D. \end{aligned} \tag{3.21}$$

3.1.2.4 Output Diodes Current

The current waveform of the output diodes is depicted in Fig. 3.6. By applying an approximation one can calculate the diode current equal to half of the output inductor current during the power transfer time. The average current of the output diode current can be calculated as [15]

$$I_D = [\frac{1}{2}(I_{1S} + I_{PS}) D \frac{T_s}{2} + \frac{1}{2} I_{PS}(1 - D) \frac{T_s}{2}]/T_s. \tag{3.22}$$

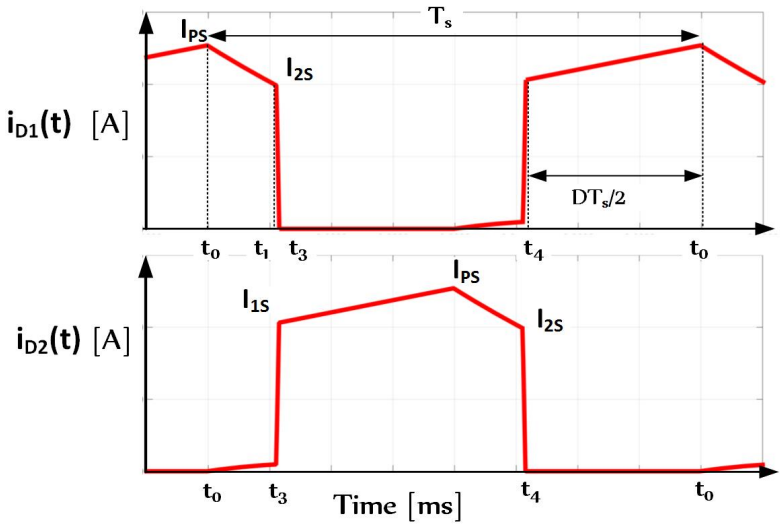

Figure 3.6: The current waveform of the output diodes

3.1.2.5 The Mosfet Switch RMS Current

By selecting proper Mosfets, the switching loss of the components is in principle zero. The body diode of the Mosfet conducts the current for a short time during the transition, but with a proper approximation, the effect of this current can be neglected. The current of the Mosfet during the power transfer can be considered to be the same as the transformer primary current. Fig. 3.7 shows this approximation for the Mosfet current during the power transfer. The RMS current of each Mosfet switch can be expressed as [15]

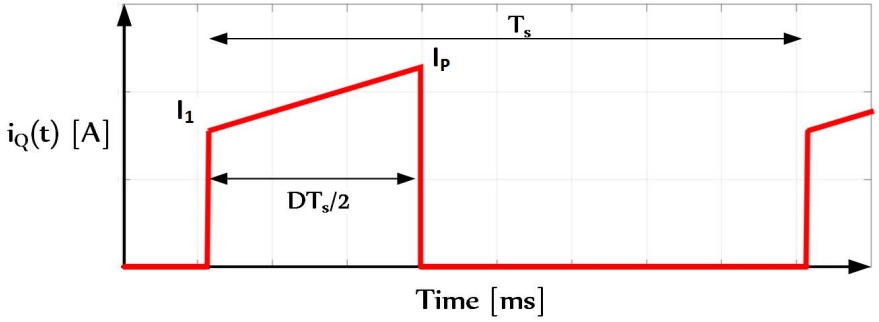

Figure 3.7: The approximation of the Mosfet current

$$I_{Mos,rms} = \sqrt{\frac{(I_P - I_1)^2 D}{6} + \frac{I_1(I_P - I_1)D}{2} + \frac{I_1^2 D}{2}}. \tag{3.23}$$

3.1.3 Zero Voltage Switching Range

As mentioned before, the right leg switches of the converter always have ZVS operation, but for the left leg switches of the converter, by considering two conditions ZVS operation can be obtained. First, there should be enough stored energy in the leakage inductance in order to conduct the current through the output capacitance of the switches to de-charge and charge them. From the mentioned equation in (3.3), the critical current in the primary of the transformer for the ZVS operation is as [15]

$$I_{crit} = \sqrt{\frac{C_R.V_{idc}^2}{L_R}} \tag{3.24}$$

where $C_R = \frac{8}{3}C_{oss} + C_T$

and C_{oss} is the switch output capacitance, C_T is the transformer winding capacitance, L_R is the transformer leakage inductance, and V_{idc} is the input voltage. The ZVS achieves for the condition where the primary current of the transformer (I_2) at t_2 or t_6 is higher than the critical current.

The second condition for the ZVS operation is enough dead time for the transition between Q_A and Q_B to ensure that the output capacitor of the switch Q_B discharge completely and then the switch diode D_B conducts current before Q_B turns on and the same for Q_A. However, with a long dead time, the output capacitor of the switch will discharge and continue to resonate and then drop. The resonance between L_R, C_{oss}, and C_T provides a sinusoidal voltage across the switch capacitance which reaches its peak value at one fourth of the resonance period, that can be expressed as [15]

$$T_{max} = \frac{T}{4} = \frac{\pi}{2}\sqrt{L_R.C_R}. \tag{3.25}$$

3.1.4 Transformer Design Parameters for Single-phase DC/DC Converter

The transformer is used to perform voltage transformation, step up or down the voltages in the power system, and provide galvanic isolation within its primary and secondary terminal. The transformer equivalent circuit for a high frequency analysis consists of: an ideal transformer (N_p, N_s), loss components (R_p, R_s, R_{core}), magnetizing inductance (L_m) and parasitic components, leakage inductance and input capacitance (L_{leak}, C_T).

3.1.4.1 Number of Turns in the Primary and Secondary Windings

Faraday's law gives a relation between voltage, flux density, and frequency as

$$V_p = 4N_pA_cB_mf_s \tag{3.26}$$

where
V_p is the voltage applied to the primary winding (V)
N_p is the number of the primary turns
A_c is the core cross section area (m^2)
B_m is the maximum flux density (T)
f_s is the frequency of operation (Hz).

The flux density is chosen as a maximum value, which should be less than the saturation value to get a smaller size of the core with smaller number of turns. Cost and size of the transformer must be considered in the design of the transformer, which is related to B_m, N, and A_c optimization. From (3.26) the number of turns in the primary can be calculated.

The relation between the primary and secondary is expressed in (3.27). By using the equation between the primary and secondary, the number of turns in the secondary of the transformer can be calculated as

$$\frac{V_p}{V_s} = \frac{N_p}{N_s} \tag{3.27}$$

where, N_p is the number of the primary turns, N_s is the number of the secondary turns, V_p is the voltage applied to the primary winding (V), and V_s is the voltage applied to the secondary winding (V).

3.1.4.2 The Size of a Conductor

The main limiting factor for the size of a conductor is the heat creation of the conductor. The current density is related to the temperature of the conductor. By increasing the current density further, the copper losses will increase and thereby the heating, which might damage the insulation properties. The current density is defined as

$$\delta = \frac{I_{rms}}{A_{cu}} \tag{3.28}$$

where I_{rms} is the RMS value of the current and A_{cu} is the cross section area of the conductor which is obtained by

$$A_{cu} = \frac{\pi D^2}{4}. \tag{3.29}$$

For alternating currents (AC), by increasing the frequency, skin effect and proximity effect causes the winding's resistance to increase, and therefore the losses increases. At high frequencies, the resistance ratio is large, which causes the current carried by the conductor to be concentrated close to the surface. By applying an approximation, the ac resistance of the conductor can be the same as the dc resistance by considering a thickness, termed the skin depth, around a hollow conductor [19]. The skin depth is defined as

$$\delta_s = \frac{1}{\sqrt{\pi f \mu \sigma}} \tag{3.30}$$

where μ is permeability (H/m), f is frequency (Hz), and σ is conductivity (mho/m). For a copper wire at $20°C$, the skin depth is

$$\delta_s = \frac{6.6}{\sqrt{f}} \quad cm. \tag{3.31}$$

One of the methods to reduce the skin effect and proximity effect is using a litz wire, which consists of many thin wire strands, individually insulated, and twisted or woven together [20]. In order to calculate the number of litz wire in a conductor, the skin depth should be determined. The area of each thin litz wire is

$$A'_{cu} = \pi \delta_s^2. \tag{3.32}$$

If $D < 2\delta_s$ then there is no need to use the litz wire, but if $D > 2\delta_s$ the litz wire has to be employed. Then the number of litz wire can be calculated as

$$N = \frac{A_{cu}}{A'_{cu}}. \tag{3.33}$$

3.1.4.3 The Resistance of the Primary and Secondary Winding

The dc resistance of a conductor is calculated by

$$R = \frac{\rho L}{A_{cu}} \tag{3.34}$$

where ρ is the resistivity of the conductor (Ω.m), L is the length of the conductor (m), and A_{cu} is the cross section area of the primary or secondary conductor (m^2).

The lenght of the conductor is calculated by

$$L = NW \tag{3.35}$$

where N is the number of the primary or secondary winding turns, W is the average perimeter of the transformer core.

3.1.5 Power-Loss Analysis for the Phase-Shift Full-Bridge DC/DC Converter

In order to optimize the efficiency of the PSFB converter, it is necessary to calculate the power losses accurately. In this section, different losses of this converter are determined as a function of the switching frequency. The power losses in each switch-mode converter are switching losses and conduction losses of the semiconductors, copper losses and core losses of the transformer.

3.1.5.1 Switching Losses

Due to the overlapping between voltage and current of the switch during the switching transition, switching loss is generated. As the PSFB is operating in ZVS condition for a specific range, the switching loss can be neglected. Although, for non-ZVS condition, switching loss can be calculated as [21]

$$P_{SW} = \frac{1}{2}(V_s I_s)(t_f + t_r) f_s + \frac{1}{2} C_{DS} V_s^2 f_s \tag{3.36}$$

where V_s and I_s are the voltage and current of the switch in the instance of the transition, t_f and t_r are the falling and rising time of the switch, and C_{DS} is the drain-source capacitor of the switch and f_s is the switching frequency.

3.1.5.2 Conduction Losses

The switch and diode conduction losses are obtained by using the following equations

$$P_{C,M} = 4R_{DS(}on)I_{Mos,rms}^2 \tag{3.37}$$

$$P_{C,D} = 4I_D V_D \tag{3.38}$$

where $R_{DS(on)}$ is the drain-source resistor of the switch, $I_{Mos,rms}$ is RMS value of the switch current obtained from (3.23), V_D is the turn-on voltage of the diode, and I_D is the averaged value of the diode's current.

3.1.5.3 Copper Losses

The copper losses for both transformer sides can be calculated as

$$P_{Cu} = I_{p,rms}^2 R_{wp} + I_{s,rms}^2 R_{ws} \tag{3.39}$$

where $I_{p,rms}$ and $I_{s,rms}$ are the RMS value of the currents of the primary and secondary side of the transformer obtained from (3.12), (3.21), and R_{wp} and R_{ws} are the resistors of the primary and secondary winding [15].

3.1.5.4 Core Losses

An empirical Steinmetz Equation is generally used for core loss calculation of the transformer, but it does not give accurate answers under nonsinusoidal excitation, since the core loss depends only on the peak value of the magnetic induction in the S.E. The improved general Steinmetz equation (IGSE) is one of the most accurate methods for core loss calculation, which extends Steinmetz Equation for non-sinusoidal waveforms. According to the IGSE the transformer core loss per unit volume is expressed as [14].

$$p_{Core} = 2^{\beta+\alpha} D^{1-\alpha} K_i f^{\alpha} B_m^{\beta} \tag{3.40}$$

and the transformer core loss is given by

$$P_{Core} = p_{Core} V_e \tag{3.41}$$

where B is the maximum flux density, K_i, α and β are the core material constants, D is the duty cycle of the signals, and V_e is the total volume of the core.

3.1.5.5 Total Losses and Efficiency

The total losses are the sum of losses of switches (conduction and switching loss), diodes (conduction loss) and transformer (core and copper losses). Therefore, the efficiency of the converter is expressed as

$$P_{loss} = P_{C,M} + P_{SW} + P_{C,D} + P_{Cu} + P_{Core} \tag{3.42}$$

$$\eta = \frac{P_o}{P_o + P_{loss}}. \tag{3.43}$$

3.2 A Three-Phase Full-Bridge DC/DC Converter with High-Frequency Isolation

A three phase DC/DC converter topology suitable for high-power applications is shown in Fig. 3.8a. The MOSFET switches are operating in soft-switched mode, which reduces the switching losses. The operation principle is very similar to the phase-shifted full-bridge (PSFB) DC/DC converter. The three-phase DC/DC converter has several advantages compared to the single phase DC/DC converter such as reducing RMS current through the MOSFET switches, higher power transfer, reduction of the filter's size due to increased switching frequency by a factor of three, reduction in transformer size due to better utilization of transformer's copper and core, reduced semiconductor stresses results in lower switching losses and consequently an increase of the efficiency [22].

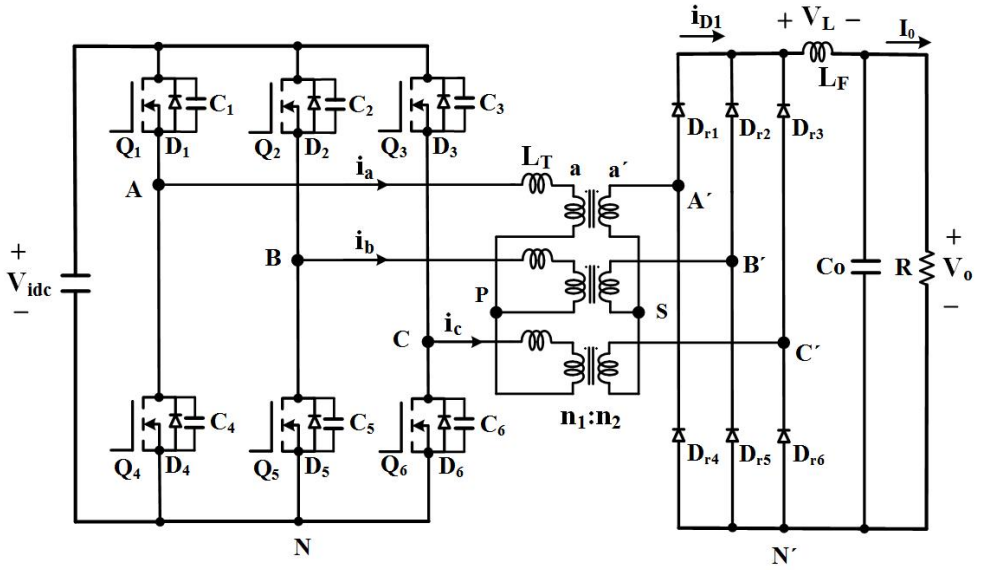

(a)

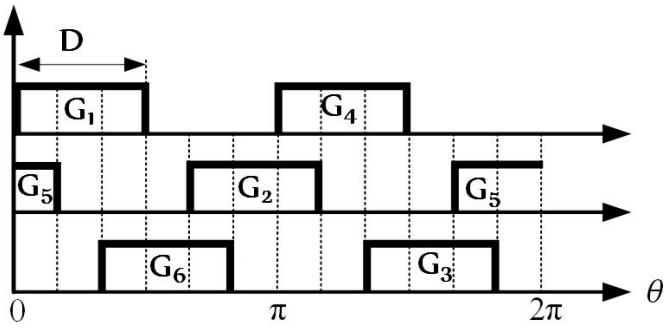

(b)

Figure 3.8: Three-phase full-bridge DC/DC converter (a) Main circuit (b) Control strategy

3.2.1 Analysis of the Three-Phase DC/DC Converter

The suggested topology uses a three-phase converter with six MOSFET switches, coupled to a three-phase high frequency transformer with Y-Y connection and to a three-phase high frequency rectifier derived from the single-phase full-bridge DC/DC converter in section 3.1 (Fig. 3.8a).

The control strategy of the semiconductor components is essential for the system's performance. In a three-phase converter circuit, each leg has a 120° phase-shift forwards each other. A single pulse PWM gate signal is utilized to control the output voltage of a three-phase converter as shown in Fig. 3.8b. The duty cycle of any switches are between 60° to 120°. If the duty cycle is less than 60° only one switch conducts and the output voltage is zero. For a duty cycle higher than 120°, there is no output voltage control. In order to get zero to full output voltage, the duty cycle is adjusted from 16.66% to 33.33% [22], [23].

3.2.1.1 Three-Phase Converter Waveforms

In order to find the waveforms of the three-phase converter, the phase voltage of the input and output of the transformer must be calculated.

$$V_{AP} + V_{BP} + V_{CP} = V_{AN} + V_{BN} + V_{CN} - 3V_{PN} = 0 \tag{3.44}$$

$$V_{PN} = \frac{V_{AN} + V_{BN} + V_{CN}}{3} \tag{3.45}$$

$$V_{AP} = V_{AN} - V_{PN} \tag{3.46}$$

$$V_{BP} = V_{BN} - V_{PN} \tag{3.47}$$

$$V_{CP} = V_{CN} - V_{PN} \tag{3.48}$$

The output phase voltage of the transformer ($V_{A'S}, V_{B'S}, V_{C'S}$) is obtained by using the transformer turns-ratio. The gate signals and the waveforms of the three-phase full-bridge dc-dc converter are depicted in Fig. 3.9.

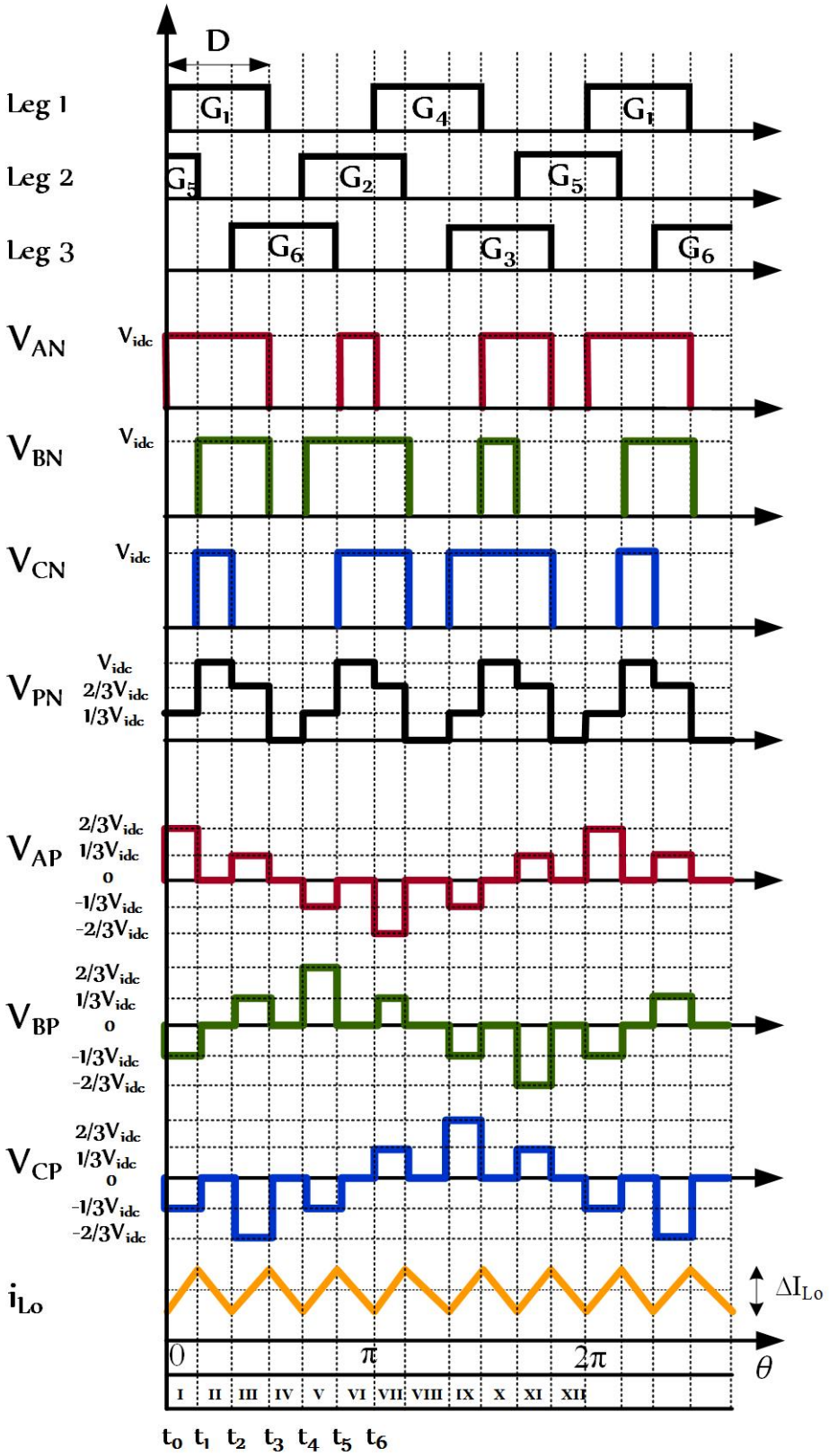

Figure 3.9: The waveforms of three-phase full-bridge DC/DC converter

3.2.1.2 Principles of Operation

The three-phase full-bridge converter which is illustrated in Fig. 3.8a is considered for analyzing the variety of modes of circuit operation. By employing the maximum input dc voltage and a duty cycle less than 33.33%, it is observed that in each time interval either two transistor switches from two phases with the body diode of the transistor in the third phase or one transistor switch and two body diodes of the transistors in the second and third phase are conducting in the circuit.

When two transistor switches are conducting, one switch is on from the upper switch group (Q_1, Q_2 and Q_3) and one other from the lower switches group (Q_4, Q_5 and Q_6) is on. In this case, two of the transformer primary terminals are connected to the dc supply and the potential of the terminals are known. The third terminal of the transformer is connected by the body diode of the transistor which remains floating and the potential of the third terminal depends on the condition of the high-frequency link parameters.

Fig. 3.9 shows the waveforms of the three-phase converter. In time interval I switches Q_1 and Q_5 are conducting. In the secondary side of the transformer the rectifier diodes D_{r1} , D_{r3} and D_{r5} are connected. The output current I_o increases with a rate obtained by the difference between the input voltage V_i/n and the load voltage V_o. (The transformer turn-ratio n is equal n_1/n_2).

In time interval II, switch Q_5 is turned off, switch Q_1 is still on and current i_a transfers through body diodes D_2 and D_3. In the output of the converter, all six rectifier diodes conduct the output current I_o and the voltage on the secondary side of transformer is zero. During this time interval switch Q_1 and body diodes D_2 and D_3 are conducting the current i_a. By considering ideal condition and neglecting the forward voltage drop over transistors the current i_a is constant at the end of this time interval.

In interval III, switch Q_6 is turned on and current i_a is transferred through switches Q_1, Q_6 and body diode D_2. In the secondary side of the transformer the output current I_o is transferred through the rectifier diodes D_{r1}, D_{r5} and D_{r6}. In time interval IV, switch Q_1 is turned off and switch Q_6 is still conducting. Current i_a is forced to transfer through switch Q_6 and body diodes D_4 and D_5. In the secondary side all the rectifier diodes are conducting the output current I_o.

In time interval V, switch Q_2 is connected and current i_b is commuted through switch Q_2 and switch Q_6. At this instant, voltage and current are shifted from one phase to next phase. In this time interval, switches Q_2, Q_6 and body diode D_4 are conducting the current i_b. In the secondary side of the transformer the output current I_o is transferred through rectifier diodes D_{r1}, D_{r2} and D_{r6}.

Table 3.1: Sequence of Operation of a Three-Phase Converter

Mode	***Gate signals***	***Primary side***	***Secondary side***
I, t0<t<t1	G1, G5	Q1, Q5, D6	Dr1, Dr3, Dr5
II, t1<t<t2	G1	Q1, D2, D3	Dr1 to Dr6
III, t2<t<t3	G1, G6	Q1, D2, Q6	Dr1, Dr5, Dr6
IV, t3<t<t4	G6	D4, D5, Q6	Dr1 to Dr6
V, t4<t<t5	G2, G6	Q2, D4, Q6	Dr1, Dr2, Dr6
VI, t5<t<t6	G2	D1, Q2, D3	Dr1 to Dr6
VII, t6<t<t7	G2, G4	Q2, D3, Q4	Dr2, Dr4, Dr6
VIII, t7<t<t8	G4	Q4, D5, D6	Dr1 to Dr6
IX, t8<t<t9	G3, G4	Q3, Q4, D5	Dr2, Dr3, Dr4
X, t9<t<t10	G3	D1, D2 ,Q3	Dr1 to Dr6
XI, t10<t<t11	G3, G5	D1, Q3, Q5	Dr3, Dr4, Dr5
XII, t11<t<t12	G5	D4, Q5, D6	Dr1 to Dr6

In time interval VI, switch Q_6 is disconnected and the current i_b is commuting through switch Q_2 and body diodes D_1 and D_3. In the secondary side of the transformer like the previose stage all the rectifier diodes are conducting and the voltage over primary and secondary side of transformer are zero. The sequence of switches and diodes of the converter in one period of circuit operation is depicted in Table. 3.1. The equivalent circuit of the three phase converter in each time intervals is shown in Fig. 3.10.

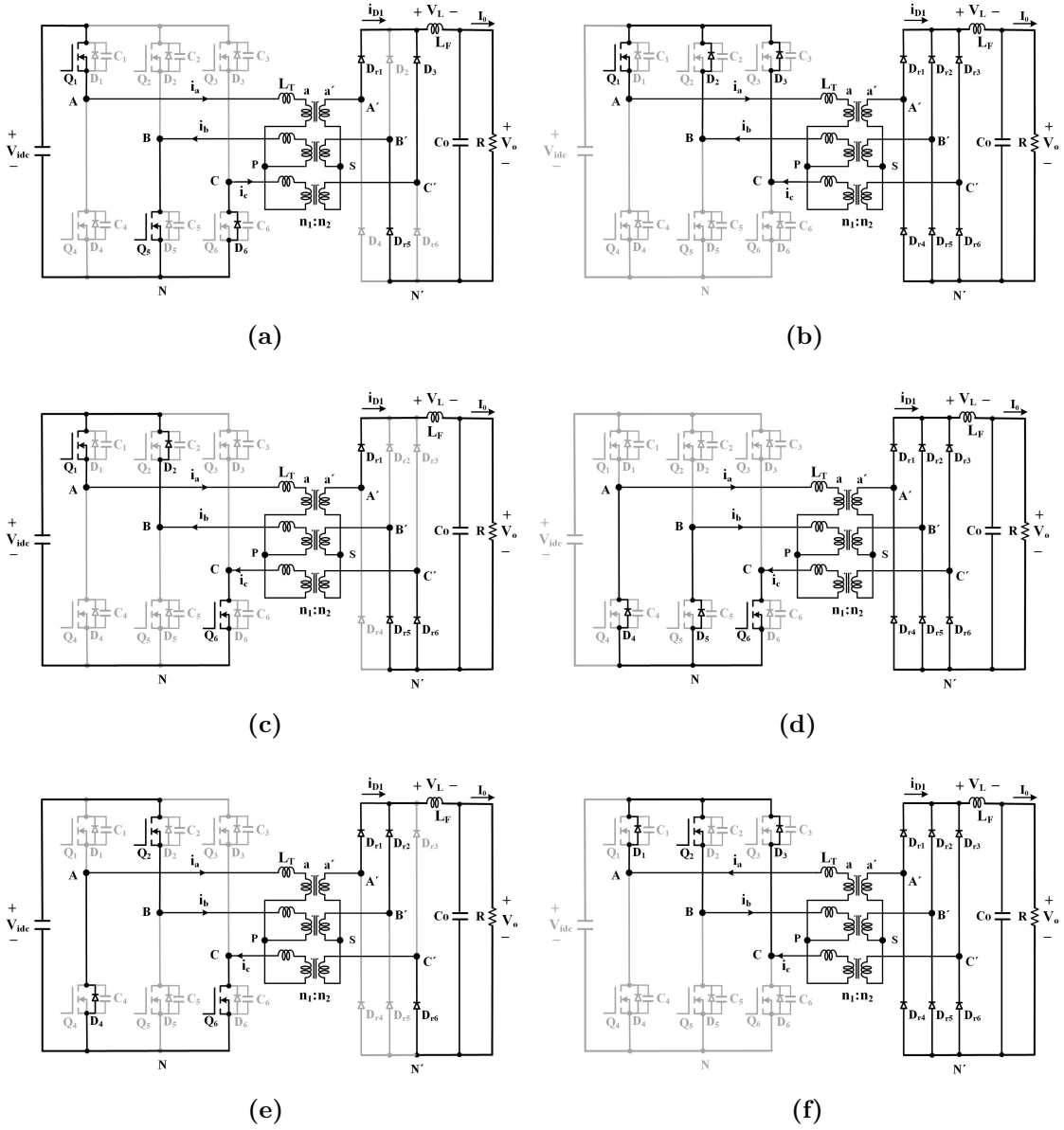

Figure 3.10: Operation of the Three-Phase Full-Bridge Converter
(a) The power transfer interval $t_0 < t < t_1$ (b) The time interval $t_1 < t < t_2$
(c) The power transfer interval $t_2 < t < t_3$ (d) The time interval $t_3 < t < t_4$
(e) The power transfer interval $t_4 < t < t_5$ (f) The time interval $t_5 < t < t_6$

3.2.1.3 The Input/Output Voltage Relation

By considering the current waveform of the output inductor, and the position of the primary switch gates, the relation between input and output voltage can be evaluated. As is shown in Fig. 3.11 during ΔT_1 two gates of the primary switches are on, and the current in the secondary side is charging the output inductor. During ΔT_2 just one gate of the primary switches is on, and that makes one switch and two other diodes to circulate the current in the primary circuit. Then in the secondary side all the six rectifier diodes conduct which causes a short circuit over secondary side of the transformer, and the output inductor discharges during ΔT_2 by the load. As the voltage of the output inductor during this time interval (ΔT_1+ΔT_2) is zero then by applying those time intervals' equations the input and output relation is find out [24].

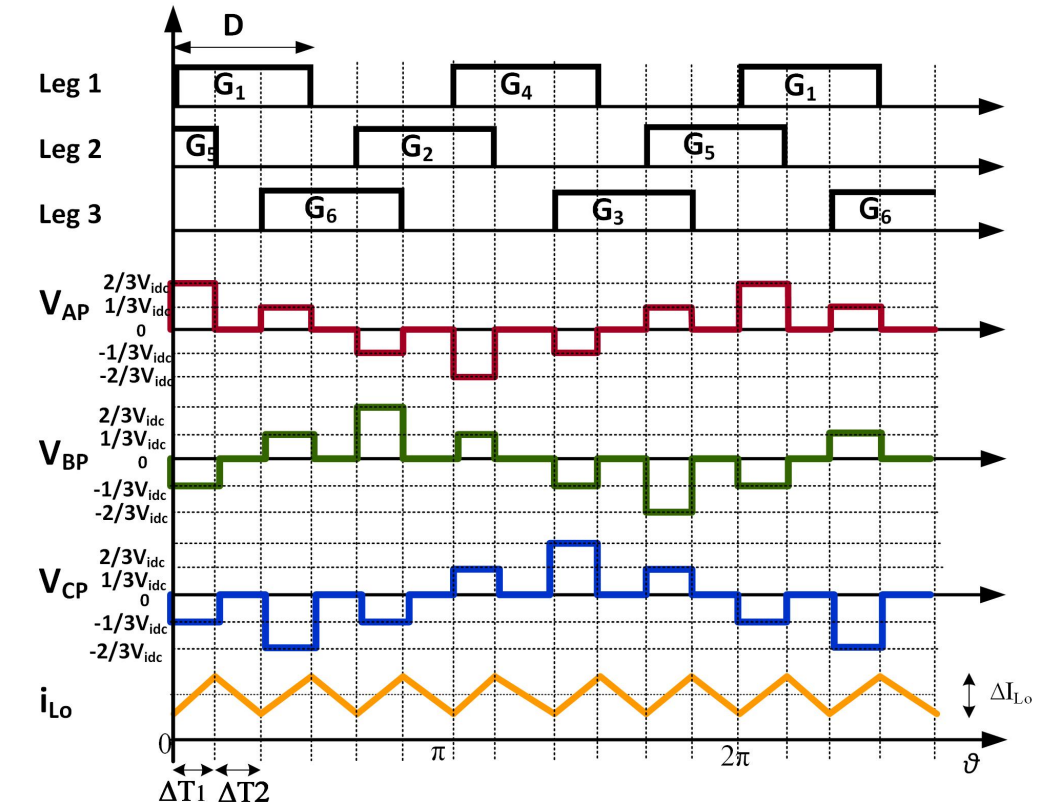

Figure 3.11: The waveforms of the input voltages and current of output inductor

$$\Delta T_1 = (D - \frac{1}{6})T_s \tag{3.49}$$

$$\Delta T_2 = (\frac{1}{3} - D)T_s \tag{3.50}$$

$$\int_0^{\Delta T_1 + \Delta T_2} V_L dt = 0 \tag{3.51}$$

By solving (3.51) the following result is found.

$$(\frac{V_{in}}{n} - V_{out})(D - \frac{1}{6})(T_s) + (-V_{out})(\frac{1}{3} - D)(T_s) = 0$$

$$\frac{V_{out}}{V_{in}} = \frac{6D - 1}{n} \tag{3.52}$$

3.2.2 Phase Current Waveforms

As observed from Fig. 3.11 and Fig. 3.12 during duty cycle D switch Q_1 is on and in phase a the current in this time interval ($T^{'}$) is the output current transferred to the primary side with the transformer's turn ratio ($1/n$). After switch Q_1 turns off, at 120° switch Q_2 in the second phase turns on. Between turning off switch Q_1 and turning on switch Q_2, which is time interval $T^{''}$, diode D_4 is on which is coincident with the time that in the secondary side all the rectifier diodes are conducting and there is short circuit over the transformer. Then in the primary side, the current in phase a continues to circulate in the same direction among diodes D_4, D_5 and switch Q_6. It is concluded that in the time interval $T^{'} + T^{''}$ for 120° the current in the primary is positive [24].

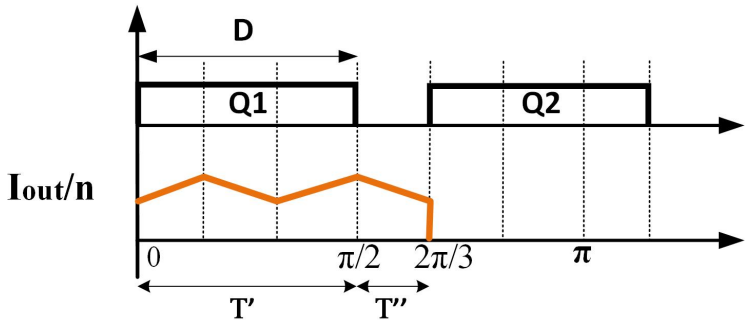

Figure 3.12: The waveforms of the primary switches and input current

The same procedure will happen, but with negative current after 180°. At 180° switch Q_4 is on during the duty cycle, after turning off switch Q_4, the upper diode D_1 is on to keep the negative current circulating for the time equal to 120°. The current in phase b and c is the same with a delay of 120° for each. It is concluded that for every duty cycle between 60°$<D<$ 120°, the current waveform is positive for 120° and negative for the same time. By considering a large output inductor and low voltage drop, the current during time interval $T^{'}+T^{''}$ can be supposed as a constant current, which is equal to I_{out}/n. Fig. 3.13 shows the current in the primary side of the converter for one phase (a).

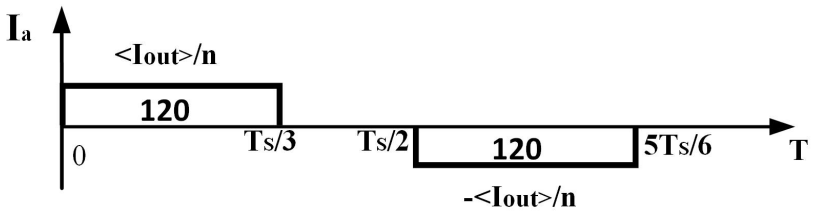

Figure 3.13: The waveforms of the input current for phase a

3.2.2.1 RMS Current of Components

1- The Transformer Primary RMS Current

$$I_{P,rms} = \frac{< I_{out} >}{n}\sqrt{\frac{2}{3}} = \frac{V_{out}}{nR_{load}}\sqrt{\frac{2}{3}} \tag{3.53}$$

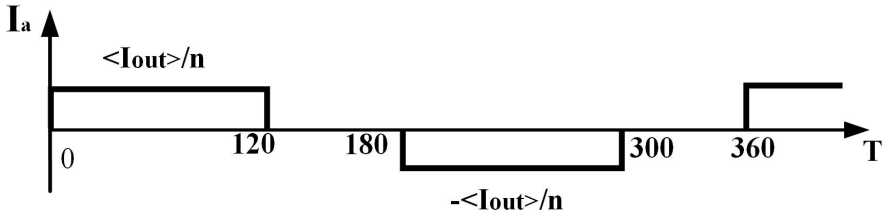

Figure 3.14: The waveforms of the transformer primary current

2- The Transformer Secondary RMS Current

$$I_{S,rms} = < I_{out} >\sqrt{\frac{2}{3}} = \frac{V_{out}}{R_{load}}\sqrt{\frac{2}{3}} \tag{3.54}$$

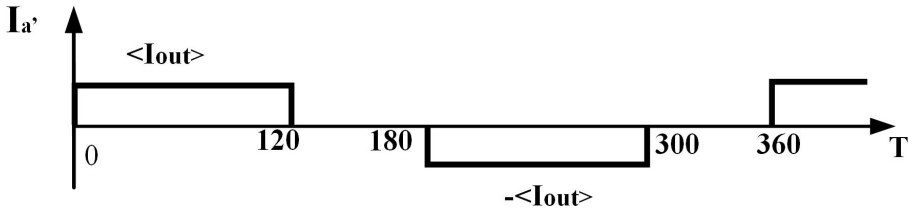

Figure 3.15: The waveforms of the transformer secondary current

3- The Mosfet Switch RMS Current
The duration for each switches to be on is equal to D.

$$I_{Mos,rms} = \frac{< I_{out} >}{n}\sqrt{D} = \frac{V_{out}}{nR_{load}}\sqrt{D} \tag{3.55}$$

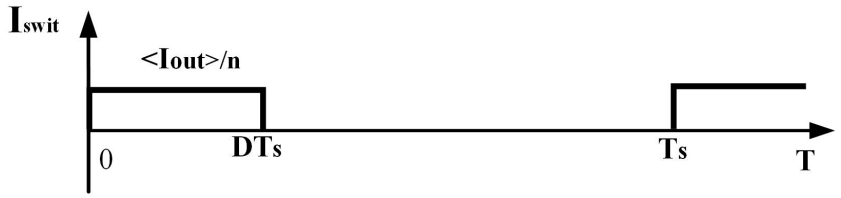

Figure 3.16: The waveforms of the input Mosfet switch's current

3.2.2.2 Average Current of Components

1- Average Current of the Output Diode of the Switch

$$I_{D_{Mos},ave} = \frac{< I_{out} >}{n}(\frac{1}{6} - D) = \frac{V_{out}}{nR_{load}}(\frac{1}{6} - D) \tag{3.56}$$

2- Average Current of Rectifier Diodes
Each of the rectifier diodes has the same current of input switches, just with the maximum average output current.

$$I_{D_{Rec},ave} = < I_{out} > \frac{1}{3} = \frac{V_{out}}{R_{load}}\frac{1}{3} \tag{3.57}$$

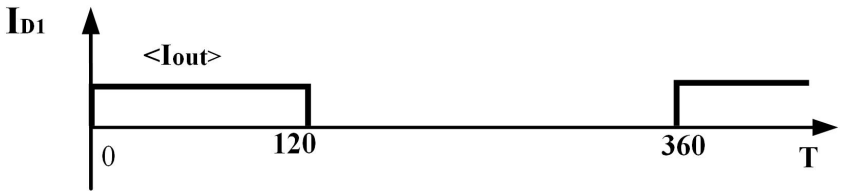

Figure 3.17: The waveforms of the rectifier diode's current

3.2.3 Mosfet Switches Behavior During Turn on and off

3.2.3.1 Turn on the Switch

In the primary side of the bridge, a leakage induuctance L_a acts as a turn-on snubber for the Mosfet switch, which is used to reduce voltage across the Mosfet while the current builds up during turn on. Due to the leakage inductance, the current change is not suddenly and has a limited slope which provides zero-current-switching for the Mosfet, which reduces the power losses during turn-on. For describing the switches behavior during turn on, switch Q_1 in phase "a" is considered. Before turning on Q_1, Q_5 and diodes D_4 and D_6 are on as Fig. 3.18 shows. On the secondary side of the bridge all the rectifier diodes are conducting. During this time interval the voltage across the secondary side of the transformer is zero which induces zero voltage in the primary side of the transformer.

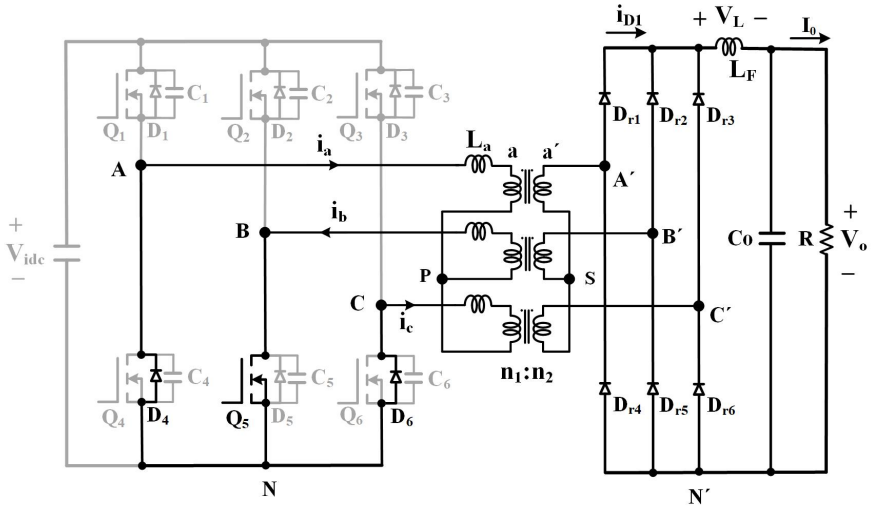

Figure 3.18: Operation of the three-phase converter before turn on Q_1

After turning on switch Q_1, the current of the leakage inductance L_a, increases with a constant $\frac{di}{dt}$. The current changes in this time interval can be calculated as [24]

$$\Delta V = L_a \frac{\Delta i_a}{\Delta t}$$

$$i_a(t) = \frac{V_{dc} t}{L_a}. \tag{3.58}$$

The current i_a continues to flow through the leakage inductance L_a, until it reaches the peak value of the current transferred from the secondary side of the bridge (i_f). This time interval after turn on of switch Q_1 is shown in Fig. 3.19

$$i_a(t) = \frac{i_f}{n} = \frac{V_{dc} t_{t1}}{L_a} \tag{3.59}$$

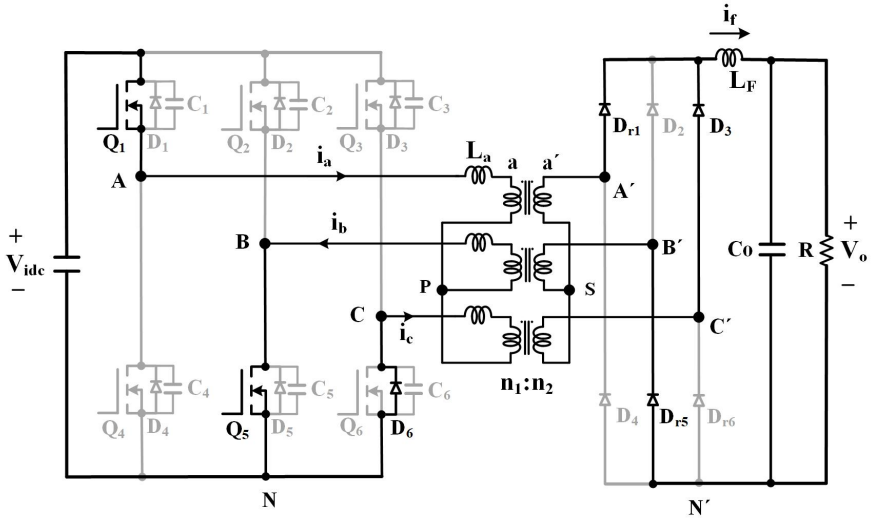

Figure 3.19: Operation of the three-phase converter after turn on Q_1

Then the required time for charging the leakage inductance can be achieved as

$$t_{t1} = \frac{i_f L_a}{V_{dc} n}. \tag{3.60}$$

3.2.3.2 Turn off the Switch

It has been considered that the Mosfet switch has a turn-off snubber, which is used to provide a zero- voltage-switching across the transistor while the current turns off. At turn-off, in the presence of this snubber capacitor, The transistor's current flows into the capacitor and start charging it to a specified level. Then the voltage across the transistor does not have sharp changes, which leads to reduction of power losses during turn off.

In order to describe the converter's behavior during turn off, Q_1 in phase "a" is considered. Before turning off Q_1, in the primary side of the bridge, Q_1, Q_6 and body diode D_2 are conducting. In the secondary side of the bridge, rectifier diodes D_{r1}, D_{r5} and D_{r6} are conducting. It is considered that the output capacitor C_1 across Q_1 is discharged and in the same leg, the output capacitor C_4 across Q_4 is charged equal to the input voltage as is shown in Fig. 3.20.

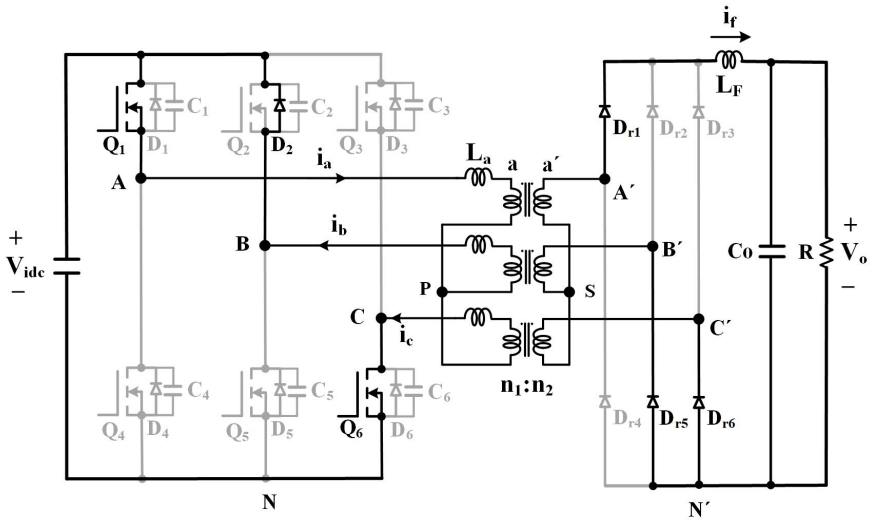

Figure 3.20: Operation of the three-phase converter before turn off Q_1

After turning off Q_1, current i_a flows through these two capacitors (C_1 and C_4), then capacitor C_1 is charged and capacitor C_4 is discharged. If the two capacitors supposed to be similar, the time interval required for charging and discharging these capacitors will be

$$t_{t2} = \frac{2CV_{dc}}{i_a}. \tag{3.61}$$

Due to the presence of the snubber capacitor in the circuit, the voltage across the Mosfet does not have sharp changes during turn off, and it increases with a constant ratio. Then it can be considered that the switch has a turn-off snubber which leads to zero-voltage-switching in turn off and the power losses can be considered as zero.

3.2.4 Transformer Design Parameters for Three-Phase DC/DC Converter

According to the Faraday's law, the RMS voltage of primary side of the transformer is

$$V_{Prms} = 4.44 N_p A_c B_m f_s \tag{3.62}$$

where V_{Prms} is the RMS voltage applied to the primary winding (V)
N_p is the number of the primary turns
A_c is the core cross section area (m^2)
B_m is the maximum flux density (T)
f_s is the frequency of operation (Hz).

As it is described in the 3.2.1.1 the voltage in each phase of the transformer in the primary side of the bridge is as Fig. 3.21.

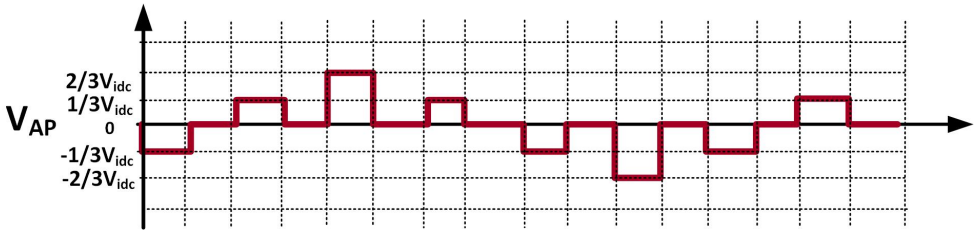

Figure 3.21: Operation of the three-phase converter after turn on Q_1

which can be considered as a sinusoidal wave with peak value equal to $\frac{2}{3}V_{dc}$ in the analysis. Then the RMS voltage of the transformer is found as

$$V_{prms} = \frac{\frac{2}{3}V_{dc}}{\sqrt{2}} = \frac{\sqrt{2}}{3}V_{dc} = 4.44N_pA_cB_mf_s. \tag{3.63}$$

From (3.63), by applying the transformer's size and the flux density, the number of turns in the primary side of the transformer can be calculated. Then by using the transformer turn-ratio, the number of turns in the secondary side of the transformer is obtained.

$$\frac{N_s}{N_p} = \frac{V_s}{V_p} = \frac{1}{n} \tag{3.64}$$

The calculation of the wires resistance is the same as is described in the single phase in 3.1.4.3.

3.2.5 Evaluation of Different Losses in the Three-Phase Converter

3.2.5.1 Switching Losses

Due to the presence of turn-on and turn-off snubbers, which was described in 3.2.3, the switching losses can be considered as zero.

3.2.5.2 Conduction Losses of the Mosfet Switch

$$P_{C,M} = 6R_{DS}(on)I^2_{Mos,rms} \tag{3.65}$$

3.2.5.3 Conduction Losses of the Body Diode of the Switch

$$P_{C,MD} = 6V_{D_M}(on)I_{D_{Mos},ave} \tag{3.66}$$

3.2.5.4 Conduction Losses of the Rectifier Diode

$$P_{C,D} = 6V_D(on)I_{D_{Rec},ave} \tag{3.67}$$

3.2.5.5 Copper Losses of the Transformer

The copper losses of the transformer is the same as is described in single phase converter in 3.1.5.3.

$$P_{Cu} = 3(I_{P,rms}^2 R_{wp} + I_{S,rms}^2 R_{ws}) \tag{3.68}$$

where $I_{P,rms}$ and $I_{S,rms}$ are the RMS value of the currents of the primary and secondary side of the transformer, and R_{wp} and R_{ws} are the resistors of the primary and secondary winding.

3.2.5.6 Core Losses of the Transformer

The improved general Steinmetz equation (IGSE), is used for core loss calculation of the transformer. According to the IGSE the transformer core loss per unit volume is expressed as [14].

$$P_v = \frac{K_i}{T}\int_0^T |\frac{dB}{dt}|^{\alpha}|\Delta B|^{\beta-\alpha}dt \tag{3.69}$$

and the transformer core loss is given by

$$P_{Core} = P_v V_e \tag{3.70}$$

where B is the maximum flux density, K_i, α and β are the core material constants, and V_e is the total volume of the core.

According to Faraday's law, the flux density of the magnetic core can be achieved by integrals over the voltage of each phase of the transformer. The voltage of each phase of the transformer as described in 3.2.1.1 is shown in Fig. 3.22. By doing the integral over the voltage, the flux density curve of the magnetic core is obtained in Fig. 3.22.

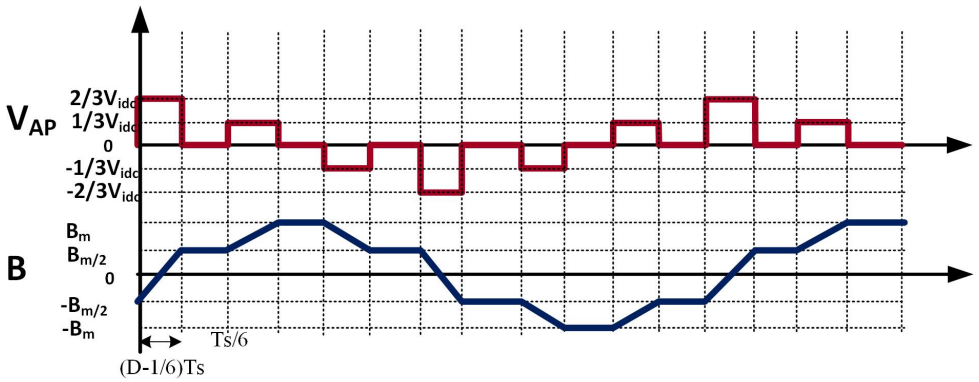

Figure 3.22: Primary voltage and flux density of the transformer

By appling (3.69), and doing the integral for each time interval the core loss per unit volume of the transformer can be achieved.

$$P_v = \frac{K_i}{T}\left(\int_0^{(D-\frac{1}{6})T_s}\left(\frac{B_m}{(D-\frac{1}{6})T_s}\right)^{\alpha} {B_m}^{\beta-\alpha} dt + \int_0^{(D-\frac{1}{6})T_s}\left(\frac{\frac{B_m}{2}}{(D-\frac{1}{6})T_s}\right)^{\alpha}\left(\frac{B_m}{2}\right)^{\beta-\alpha} dt + ...\right) \tag{3.71}$$

where for three phase transformer the core loss per unit volume will be

$$P_v = 3[2(1+2^{1-\beta})(D-\frac{1}{6})^{1-\alpha} K_i B_m^{\beta} f_s^{\alpha}] \tag{3.72}$$

and the transformer core loss is given by

$$P_{Core} = P_v V_e \tag{3.73}$$

where B is the maximum flux density, D is the duty cycle of the signals, f is the switching frequency, K_i, α and β are the core material constants, and V_e is the total volume of the core.

3.2.5.7 Total Losses and Efficiency

The total losses are the sum of losses of switches (conduction loss), diodes (conduction loss) and transformer (core and copper losses). Therefore, the efficiency of the converter is expressed as

$$P_{loss} = P_{C,M} + P_{C,MD} + P_{C,D} + P_{Cu} + P_{Core} \tag{3.74}$$

$$\eta = \frac{P_o}{P_o + P_{loss}}. \tag{3.75}$$

4

Results

In this chapter, the results of the design for a 50 kW PSFB converter and the evaluation of the converter for ZVS operation, power loss and efficiency with results of the simulation model is presented.

4.1 The Design of a 50 kW Single-Phase Phase-Shifted Full-Bridge Converter

The converter specification for the design of 50 kW system is presented in Table 4.1.

Table 4.1: Specification of the PSFB converter

Parameter	**Symbol**	**Value**
Input voltage	$Vidc$	700 V
Output voltage	V_o	250-420 V
Nominal Power	P_o	50 kW
Switching frequency	f_s	25 kHz

4.1.1 Transformer Selection

A metallic tape-wound core made of the nanocrystalline ***VITROPERM 500 F*** is used for the isolated transformer which gives very low transformer capacitance (C_T) near zero [5]. By applying (3.1), (3.2) the required transformer turn's ratio is obtained as $n = 1.2$ that gives a maximum duty cycle of around $D = 0.72$.

The specification of the transformer is defined in Table 4.2. The transformer coefficients K_i, α, and β are transformer material characteristics and can be found by datasheets.The flux density is a constant value for a whole volume of the core and is chosen by B_{max}=0.3T for the nanocrystalline VITROPERM 500 F core.

Table 4.2: Specification of the nanocrystalline VITROPERM 500F transformer

Parameter	Symbol	Value
Max. flux density	B	0.3 T
Core material constant	α	1.8
Core material constant	β	2.3
Core material constant	K_i	0.0497

4.1.2 Switch Selection

It is suggested to utilize ***1.2 kV SiC CREE*** MOSFET switches in the converter to get low switching losses. The MOSFET output capacitance (C_{oss}) of the SiC switch is $2.5nF$ according to the datasheet. The specification of the MOSFET switches is defined in Table 4.3.

Table 4.3: Specification of the half-bridge SiC modules from CREE type CAS300M12BM2

Parameter	Symbol	Value
On State Resistance	R_{ds}	5 $m\Omega$
Input Capacitance	C_{iss}	11.7 nF
Output Capacitance	C_{oss}	2.5 nF
Reverse Transfer Capacitance	C_{rss}	0.07 nF
Rise Time	t_r	68 ns
Fall Time	t_f	43 ns

4.1.3 Output Rectifier Diode Selection

In this application it is suggested to use ***300 Amp-FRED Module-600Volts*** diodes, where the maximum forward voltage of diode is $1.4V$ according to the datasheet.

4.1.4 Converter Design Calculation

In order to calculate the minimum value of the leakage inductance, it is required to consider 50% of the full load. The selection of 50% is a designer choice, it can be around (30%-70%) or similar. For a chosen condition, let say 50%, one can go ahead and perform the rest of design that is inductor selection and so on. For this reason the minimum value of the leakage inductance can be calculated as follow [15]

$$P_{50\%} = 25 \ kW \tag{4.1}$$

$$L_R = \frac{2W_L}{i_L^2} = 1 \ \mu H \tag{4.2}$$

where W_L is the leakage inductance energy which can be achieved by employing (3.3).

By considering $\triangle I_o = 0.1(I_o) = 11.9$, the magnetization inductance of the transformer can be calculated as

$$L_M \geq \frac{nDV_i}{4\triangle I_o f_s} = 600 \ \mu H. \tag{4.3}$$

Then, the output inductor is expressed as

$$L_f = \frac{V_{o,nom}(1 - D_{nom})}{4\triangle I_o f_s} = 100 \ \mu H. \tag{4.4}$$

If the output voltage ripple is supposed to be less than $1V$ ($\triangle V_o \leq 1V$), then, the output capacitor is defined as

$$C_o \geq \frac{\triangle I_o T_s}{16\triangle V_o} = 33 \ \mu F. \tag{4.5}$$

With a design procedure that presented in Section 3.1.2, the designed parameters are shown in Table 4.4.

Table 4.4: Designed parameters of the PSFB converter

Parameter	**Symbol**	**Value**
Leakage inductor	L_R	$1\mu H$
Magnetizing inductor	L_M	600 μH
Output filter	L_f	100 μH
Output capacitor	C_o	33 μF

4.1.5 Zero Voltage Switching Range

Fig. 4.1, and Fig. 4.2 provide a comparison of waveforms of the converter at two different input voltage equal to $350V$, $f_s = 25kHz$, and output power equal to $P_o = 23kW$ and $27kW$. As described previously, ZVS of the left leg of the converter is achieved for the condition when the stored energy of the leakage inductance is enough to charge and discharge the capacitances. As can be seen from Fig. 4.1 ZVS operation is achieved in the mentioned condition for the output power equal to $P_o = 27kW$, but in Fig. 4.2 the capacitors of the switches don't have enough time to charge and discharge during the dead time, then ZVS operation is lost, which is predicted by analysis when the load current is below the critical current in (3.24).

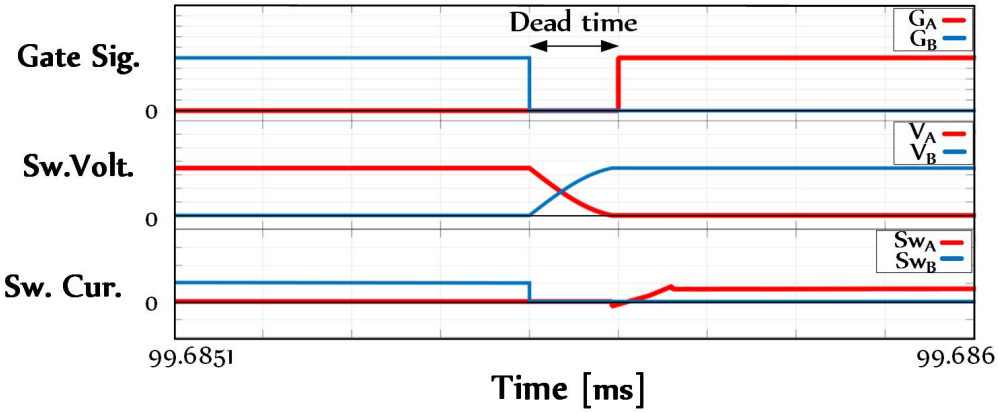

Figure 4.1: The gating signals, voltage and current waveforms of left leg switches for $V_i = 350V$, $P_o = 27kW$, $f_s = 25kHz$ with ZVS operation

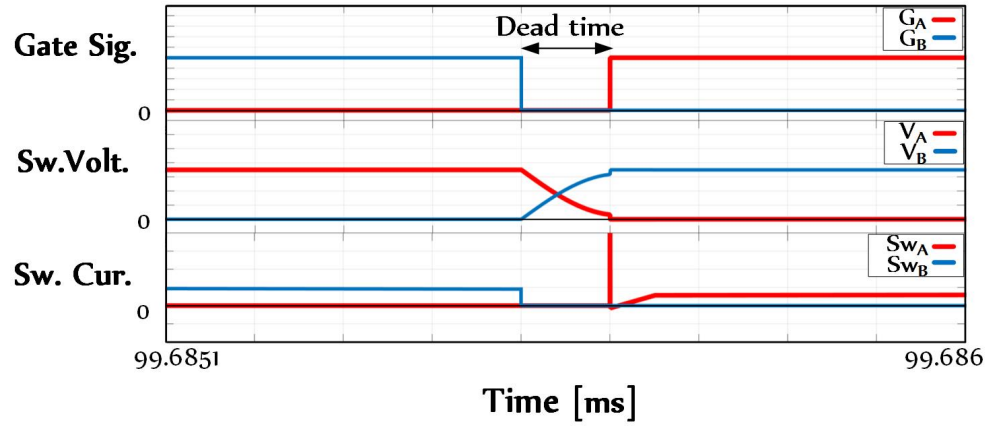

Figure 4.2: The gating signals, voltage and current waveforms of left leg switches for $V_i = 350V$, $P_o = 23kW$, $f_s = 25kHz$ without ZVS operation

By using (3.11), (3.24) the following equation (4.6) for the boundary conditions of ZVS operation is extracted. It is indicated that by increasing the frequency, if $\triangle I_o > I_M$ the P_{ZVS} increases, and if $\triangle I_o < I_M$ the P_{ZVS} decreases. In our proposed design $\triangle I_o < I_M$ then, by increasing the frequency power boundary, a wider region for ZVS operation is obtained.

$$P_{ZVS} = V_o[n(I_P - I_M) + \triangle I_o] \tag{4.6}$$

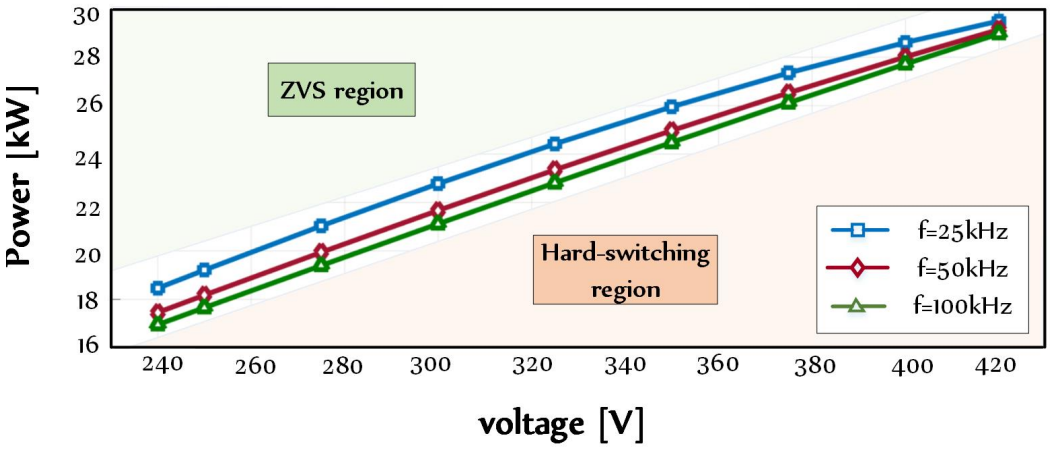

Figure 4.3: ZVS boundaries for three different frequencies

Fig. 4.3 shows ZVS operation region for three frequencies versus different output voltages for different output powers. As it is shown for $f_s = 100kHz$, the ZVS region is wider than $f_s = 25kHz$, but the drawback in this case is that by increasing the switching frequency it increases switching losses, and therefore the efficiency decreases.

4.1.6 Transformer Parameters Calculation for Single-Phase DC/DC Converter

In this part, the results of the design for the transformer parameters for a 50 kW PSFB by refereing Section 3.1.4 is presented. The converter specification for the design of 50 kW system is given as

Input voltage V_{idc}=700 V
Output voltage V_o=250 V
Nominal Power P_o=50 kW
Switching frequency f_s=25 kHz
Number of turns-ration $n = N_p/N_s$=1.2
RMS value of primary phase current $I_{p,rms}$=169.33 A

The flux density is a constant value for a whole volume of the core and is chosen by $B_{max} = 0.3T$ for the nanocrystalline VITROPERM 500 F core. The core cross sectional area (A_c) for the mentioned core is A_c=5.70 cm^2. In this design two cores as a stack (two toroidal cores) are attached to each other, in orther to make a bigger core and resulting less losses [5]. By using two cores the total weight of the magnetic core is obtained around $5kg$.

In this case the number of turns in the primary and the secondary winding is obtained by

$$N_p = \frac{V_{idc}}{4A_c B_{max} f_s} = 20 \tag{4.7}$$

$$N_s = \frac{N_p}{n} = 16. \tag{4.8}$$

4.1.6.1 Primary Winding Calculation

The next step is calculating the size of the conductor. By considering the current density for copper conductor $\delta = 5\ A/mm^2$, the cross section area of the primary conductor is obtained by

$$A_{cu,pri} = \frac{I_{p,rms}}{\delta} = 33.86\ mm^2. \tag{4.9}$$

In order to find if the litz wire will be applied and to obtain the number of litz wires, the skin depth must be calculated by

$$\delta_s = \frac{66}{\sqrt{f_s}} = 0.4174 \quad mm. \tag{4.10}$$

The diameter of the conductor is as

$$D = \sqrt{\frac{4A_{cu,pri}}{\pi}} = 6.56 \quad mm. \tag{4.11}$$

By considering $D > 2\delta_s$, the calculation for the litz wire is necessary. From the standard tables of AWG wire sizes, the proper size for the litz wire is chosen as $D_{Litz} = 0.812\ mm$ and $A'_{cu} = 0.518\ mm^2$ [25]. Then the number of the litz wire in the conductor is obtained by

$$N_{p_{litz}} = \frac{A_{cu,pri}}{A'_{cu}} = 65.38. \tag{4.12}$$

By applying the litz wire, the conductor size will be $A_{cu,pri} = 65.38x0.518 = 33.87\ mm^2$. In order to calculate the resistance of the primary winding, the length of the conductor must be determined. From the datasheet of the nanocrystalline VITROPERM 500 F core, the average perimeter of the transformer core is $w = 200mm$. Then the length of the primary conductor is obtained by $L = N_p.w = 20x0.2 = 4m$. The resistance of the primary winding is calculated as

$$R_{wp} = \frac{\rho L}{A_{cu,pri}} = 2\ m\Omega \tag{4.13}$$

where the resistivity of the copper conductor is $\rho = 1.68x10^{-8}$ (Ω.m).

4.1.6.2 Secondary Winding Calculation

The same procedure as Section 4.1.6.1 is used for the secondary winding calculation. The calculation is as

RMS value of secondary phase current $I_{s,max}$=198.05 A
The secondary conductor area $A_{cu,sec}$=$\frac{I_{s,rms}}{\delta} = 39.61\ mm^2$
The skin depth $\delta_s = \frac{66}{\sqrt{f_s}} = 0.4174\ mm$
The litz wire area $A'_{cu} = 0.518\ mm^2$
The number of litz wire $N_{s_{litz}} = \frac{A_{cu,sec}}{A'_{cu}} = 76.47$
The secondary conductor area $A_{cu,sec} = 76.47x0.518 = 39.61\ mm^2$
The length of the secondary conductor $L = N_s.w = 16x0.2 = 3.2\ m$
The resistance of the secondary winding $R_{ws} = \frac{\rho L}{A_{cu,sec}} = 1.4\ m\Omega$.

4.1.7 Total Loss Calculation for Single-Phase DC/DC Converter

Here the calculation of the total loss for the nominal output voltage in a condition without ZVS operation is presented. In order to take out the total loss diagram for different output voltages and different output powers of the converter the procedure is the same.

-The specific value of operation parameter

Input voltage $V_{idc} = 700\ V$
Output voltage $V_o = 250\ V$
Output power $P_o = 50\ kW$
Switching frequency $f_s = 25\ kHz$
Transformer turns ratio $n = 1.2$
Leakage inductance $L_r = 1\ \mu H$
Magnetizing inductance $L_m = 600\ \mu H$
Output filter inductance $L_f = 100\ \mu H$
Output filter capacitance $C_o = 33\ \mu F$

-The specific value of the MOSFET switch

Output capacitance of the switch $C_{oss} = 2.5\ nF$
Drain source capacitance of the switch $C_{ds} = 2.43\ nF$
Drain source resistance of the Switch $R_{ds} = 5\ m\Omega$
Fall time of the switch $t_f = 43\ ns$
Rise time of the switch $t_r = 68\ ns$

-The specific value of the transformer

Maximum flux density $B_{max} = 0.3\ T$
Primary winding resistance $R_{wp} = 2\ m\Omega$
Secondary winding resistance $R_{ws} = 1.4\ m\Omega$
Transformer coefficient $K_i = 0.0497$
Transformer coefficient $\alpha = 1.8$
Transformer coefficient $\beta = 2.3$

-The currents value of the converter

Duty cycle $D = \frac{nV_o}{V_i} = 0.42$
Output current $I_o = \frac{P_o}{V_o} = 200\ A$
RMS value of the primary phase current $I_{p,rms} = 169.33\ A$
RMS value of the secondary phase current $I_{s,rms} = 198.05\ A$
RMS value of the switch current $I_{mos,rms} = 77.28\ A$
Average value of the diode current $I_D = 73.46\ A$

-The different losses calculation

Rectifier diode conduction loss $P_{C,D} = 4I_D V_D = 411.42\ W$

Switch conduction loss $P_{C,M} = 4R_{DS(}on)I^2_{Mos,rms} = 119.45\ W$

Switching loss $P_{SW} = 2(\frac{1}{2}(V_s I_s)(t_f + t_r)f_s + \frac{1}{2}C_{DS}V_s^2 f_s) = 0\ W$

Transformer copper loss $P_{Cu} = I^2_{p,rms}R_{wp} + I^2_{s,rms}R_{ws} = 112.26\ W$

Transformer core loss per unit volume $p_{Core} = 2^{\beta+\alpha}D^{1-\alpha}K_i f^{\alpha}B_m^{\beta} = 34.56\ W$

Transformer core loss $P_{Core} = p_{Core}V_e = 34.56x5 = 172.82\ W$

Converter total loss $P_{loss} = P_{C,M} + P_{SW} + P_{C,D} + P_{Cu} + P_{Core} = 815.95\ W$

Converter efficiency $\eta = \frac{P_o}{P_o + P_{loss}} = 98.39\,\%$.

4.1.8 Total Losses of Single-Phase DC/DC Converter

According to (3.40), the core loss of the transformer depends on switching frequency and duty cycle of the excitation voltage waveform. For $V_{out} = 250V$ the duty cycle has its minimum value, or $D^{1-\alpha}$ is maximum. Therefore, the maximum core loss occurs in this case. The amount of core loss is constant in whole range of output power. By increasing the power level, the RMS value of leakage inductors current becomes higher. Therefore, under full load operation, conduction and copper losses are the dominant losses. At light load condition, the switching loss is added to the converter, and in the worst case it is 18% of the total losses.

Fig. 4.4 shows the loss variation of the converter in the full load, half load, and 20% of full load condition with $V_o = 420, 350, 250V$. As it can be seen in Fig. 4.4, by increasing the switching frequency, the transformer losses (consist of the copper and core losses) are the main loss and it is around 60% of the total losses.

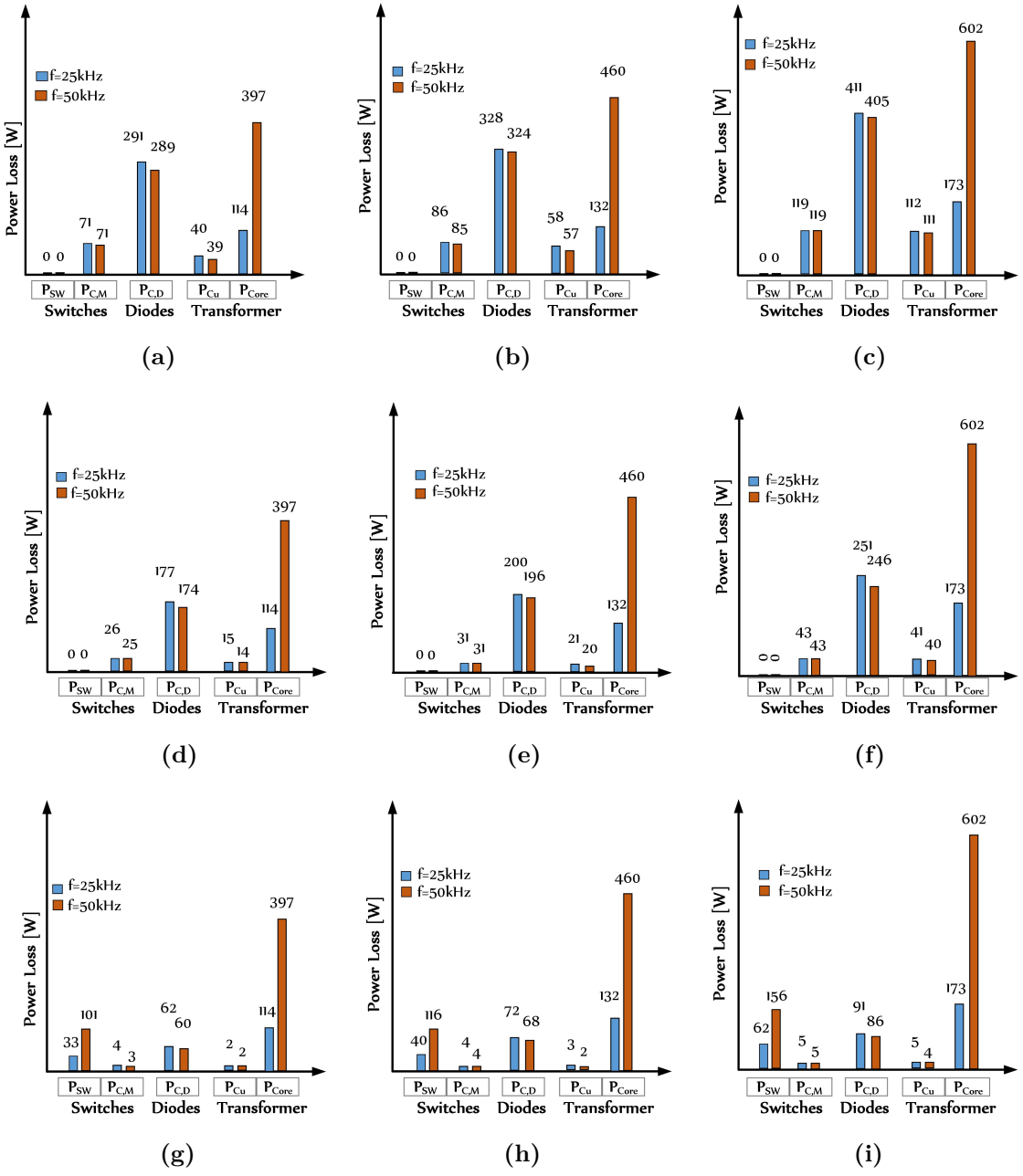

Figure 4.4: Power losses for switches, diodes and transformer
(a) $P_o = 50kW$, $V_o = 420V$ (b) $P_o = 50kW$, $V_o = 350V$ (c) $P_o = 50kW$, $V_o = 250V$
(d) $P_o = 30kW$, $V_o = 420V$ (e) $P_o = 30kW$, $V_o = 350V$ (f) $P_o = 30kW$, $V_o = 250V$
(g) $P_o = 10kW$, $V_o = 420V$ (h) $P_o = 10kW$, $V_o = 350V$ (i) $P_o = 10kW$, $V_o = 250V$

4.1.9 Efficiency of Single-Phase DC/DC Converter

Fig. 4.5 shows the efficiency of the converter for different voltages at $25kHz$ and $50kHz$. As we expected, the efficiency for 25 kHz is higher than $50kHz$, and in $50kHz$ the main losses are related to the transformer. As shown in Fig. 4.5, the efficiency in full load condition are 99% and 97.5% for $f_s = 25kHz$ and $f_s = 50kHz$, respectively. For light load condition, efficiency is reduced because of the increasing of the switching loss.

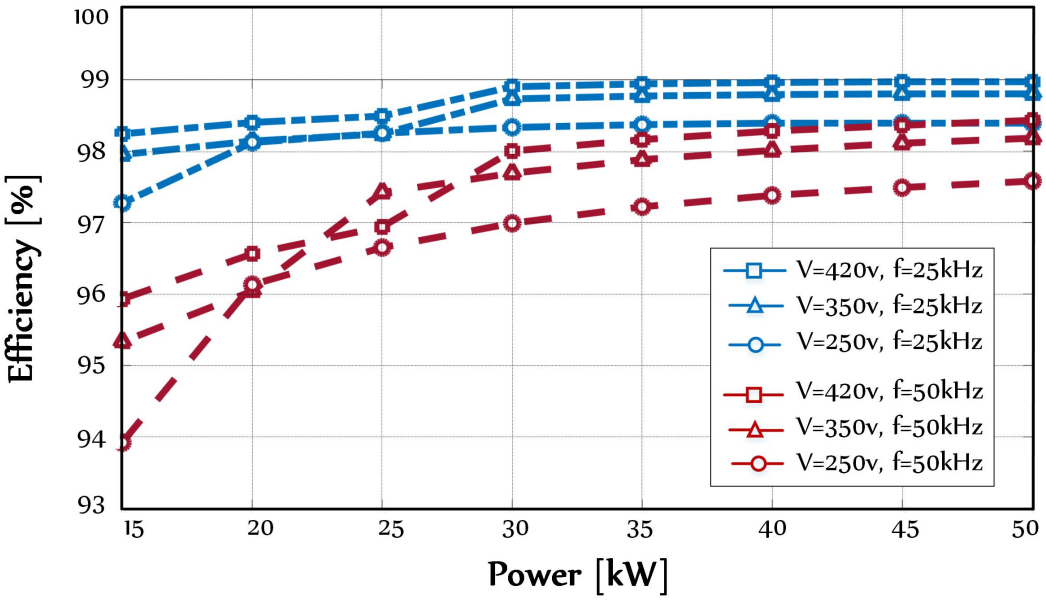

Figure 4.5: Efficiency versus power for $f_s = 25, 50kHz$

4.2 The Design of a 50 kW Three-Phase Full-Bridge DC/DC Converter

The converter specification for the design of 50 kW system is presented in Table 4.1. As the duty cycle is adjusted between $D = 60°$ and $D = 120°$, the transformer's turns ratio should be selected in order to provide the output voltage ranges between $250V$ to $420V$. By applying the voltage ratio in (3.52), the transformer's turns ratio can be selected as

$$250V \leqslant V_{out} = (\frac{6D-1}{n})V_{in} \leqslant 420V \tag{4.14}$$

$$(\frac{6D_{max}-1}{V_{out_{max}}})V_{in} = n \tag{4.15}$$

$$(\frac{6D_{min}-1}{n})V_{in} = V_{out_{min}} \tag{4.16}$$

By applying (4.15) and (4.16) the transformer's turns ratio is obtained as $n = 1.67$, and minimum duty cycle of the converter is $D_{min} = 0.2659$.

4.2.1 Design of the Leakage Inductance (L_a)

In Section 3.2.3.1 it has been discussed that the leakage inductance provides zero-current-switching for the Mosfet switch, which reduces the power losses during turn-on.The relation between different parameters during switching transient is defined in (3.59). In order to have a certain amount of changes in the current of the leakage inductance, it is desired to have the leakage inductance smaller than a specific amount.

$$L_a \leqslant \frac{t_{max}V_{dc}}{i_f/n} \leqslant 3\mu H \tag{4.17}$$

In this case the leakage inductance is selected as $L_a = 2\mu H$.

4.2.2 Design of the Magnetization Inductance (L_m)

It is same as the design for the single phase case, presented in Sections 3.1.2.3 and 4.1.

4.2.3 Design of the Output Filter Inductance

The current waveform of the output filter contains 6 pulses in each period of the switching of the full bridge converter, which includes charging and discharging of the output filter inductance for every Δt_1 and Δt_2, that has been discussed in Section 3.2.1.3. In order to have a small range of ripple in the output current, the output filter inductance is designed as

$$\Delta I \leqslant \%10 I_f \tag{4.18}$$

$$\frac{\Delta t_2 V_{out}}{L_f} \leqslant 20A \tag{4.19}$$

$$L_f \geqslant \frac{(1/3 - D_{min}) T_s V_{out_{min}}}{\Delta I} = 33.72\mu H \tag{4.20}$$

then the output filter inductance is selected as $L_f = 50\mu H$.

4.2.4 Design of the Output Capacitance

The output capacitance should have the ripple current of the output inductance in a certain range of the output voltage changes. By considering $\Delta V_{out} = \%1V$, then the out output capacitance can be obtained as

$$C_o \geqslant \frac{\Delta I \Delta t}{\Delta V_{out}} = 12.84\mu F. \tag{4.21}$$

In order to be on the safe side, $C_o = 25\mu F$.

4.2.5 Transformer Selection

The transformer selected for three phase DC/DC converter is same as the one that is chosen for single phase converter, presented in Section 4.1.1. In this work, a bank of three single-phase transformers are selected for three-phase DC/DC converter. The flux density is assumed to be a constant value for the whole volume of the core and is chosen to be B_{max}=0.3T for the nanocrystalline VITROPERM 500 F core. The core cross sectional area (A_c) for the mentioned core is A_c=5.70 cm^2 [5].

4.2.6 Transformer Parameters Calculation for Three-Phase DC/DC Converter

The converter specification for the design of 50 kW system is given as

Input voltage V_{idc}=700 V
Output voltage V_o=250 V
Nominal Power P_o=50 kW
Switching frequency f_s=25 kHz
Number of turns-ration $n = N_p/N_s$=1.67
RMS value of primary phase current $I_{p,rms}$=97,78 A

4.2.6.1 The Number of Turns in the Primary and Secondary Winding of the Transformer

By considering (3.63), the number of turns can be calculated as

$$N_p = \frac{\sqrt{2}}{3}\frac{V_{idc}}{4.44 A_c B_{max} f_s} = 18 \tag{4.22}$$

and

$$N_s = \frac{N_p}{n} = 11 \tag{4.23}$$

4.2.6.2 Resistance of the Primary Winding

The cross section area of the primary conductor is obtained as

$$A_{cu,pri} = \frac{I_{p,rms}}{\delta} = 20 \ mm^2. \tag{4.24}$$

where the current density for the copper conductor is $\delta = 5 \ A/mm^2$. The diameter of the conductor is

$$D = \sqrt{\frac{4A_{cu,pri}}{\pi}} = 5.05 \quad mm. \tag{4.25}$$

In order to find if the litz wire will be applied and to obtain the number of litz wires, the skin depth must be calculated which results in

$$\delta_s = \frac{66}{\sqrt{f_s}} = 0.4174 \quad mm. \tag{4.26}$$

By considering $D > 2\delta_s$, the calculation for the litz wire can be done. From the standard tables of AWG wire sizes, the proper size for the litz wire is chosen as

$D_{Litz} = 0.812\ mm$ and $A'_{cu} = 0.518\ mm^2$ [25]. Then the number of the litz wire in a conductor is obtained by

$$N_{p_{litz}} = \frac{A_{cu,pri}}{A'_{cu}} = 39. \tag{4.27}$$

By applying the litz wire, the conductor size will be

$$A_{cu,pri} = 39x0.518 = 20.202\ mm^2 \tag{4.28}$$

In order to calculate the resistance of the primary winding, the length of the conductor must be determined. From the datasheet of the nanocrystalline VITROPERM 500 F core, the average perimeter of the transformer core is $W = 200mm$. Then the length of the primary conductor is obtained by $L = 18x0.2 = 3.6m$. The resistance of the primary winding is calculated as

$$R_{wp} = \frac{\rho L}{A_{cu,pri}} = 3\ m\Omega \tag{4.29}$$

where the resistivity of the copper conductor is $\rho = 1.68x10^{-8}$ (Ω.m).

4.2.6.3 Resistance of the Secondary Winding

The same procedure as in Section 4.2.6.2 is used for the secondary winding calculation. The calculation is as

RMS value of secondary phase current $I_{s,rms}$=163.3 A
The secondary conductor area $A_{cu,sec}$=$\frac{I_{s,rms}}{\delta} = 32.66\ mm^2$
The skin depth $\delta_s = \frac{66}{\sqrt{f_s}} = 0.4174\ mm$
The litz wire area $A'_{cu} = 0.518\ mm^2$
The number of litz wire $N_{s_{litz}} = \frac{A_{cu,sec}}{A'_{cu}} = 64$
The secondary conductor area $A_{cu,sec} = 64x0.518 = 33.152\ mm^2$
The length of the secondary conductor $L = N_s w = 11x0.2 = 2.2\ m$
The resistance of the secondary winding $R_{ws} = \frac{\rho L}{A_{cu,sec}} = 1.11\ m\Omega$.

4.2.7 Total Loss Calculation for Three-Phase DC/DC Converter

Here the calculation of the total loss for the nominal output voltage in a condition without ZVS operation is presented. In order to take out the total loss diagram for different output voltages and different output powers of the converter the procedure is the same.

-The specific value of operation parameter

Input voltage $V_{idc} = 700\ V$
Output voltage $V_o = 250\ V$
Output power $P_o = 50\ kW$
Switching frequency $f_s = 25\ kHz$
Transformer turns ratio $n = 1.67$
Leakage inductance $L_a = 2\ \mu H$
Magnetizing inductance $L_m = 600\ \mu H$
Output filter inductance $L_f = 50\ \mu H$
Output filter capacitance $C_o = 25\ \mu F$

-The specific value of the MOSFET switch

Output capacitance of the switch $C_{oss} = 2.5\ nF$
Drain source capacitance of the switch $C_{ds} = 2.43\ nF$
Drain source resistance of the switch $R_{ds} = 5\ m\Omega$
Fall time of the switch $t_f = 43\ ns$
Rise time of the switch $t_r = 68\ ns$

-The specific value of the transformer

Maximum flux density $B_{max} = 0.3\ T$
Primary winding resistance $R_{wp} = 3\ m\Omega$
Secondary winding resistance $R_{ws} = 1.11\ m\Omega$
Transformer coefficient $K_i = 0.0497$
Transformer coefficient $\alpha = 1.8$
Transformer coefficient $\beta = 2.3$

-The currents value of the converter

Duty cycle $D = 1/6(\frac{nV_o}{V_i} + 1) = 0.26$
Output current $I_o = \frac{P_o}{V_o} = 200\ A$
RMS value of the primary phase current $I_{p,rms} = 97.78\ A$
RMS value of the secondary phase current $I_{s,rms} = 163.3\ A$
RMS value of the switch current $I_{Mos,rms} = 61.87\ A$
Average current of the output diode of the switch $I_{D_{Mos},ave} = 11.9\ A$
Average value of the rectifier diode current $I_{D_{Rec},ave} = 66.66\ A$

-The different losses calculation

Switch conduction loss $P_{C,M} = 6R_{DS(}on)I^2_{Mos,rms} = 114.85\ W$

Body diode of the switch conduction loss $P_{C,MD} = 6V_{D_M}(on)I_{D_{Mos},ave} = 85.71\ W$

Rectifier diode conduction loss $P_{C,D} = 6V_D(on)I_{D_{Rec},ave} = 560\ W$

Transformer copper loss $P_{Cu} = 3(I^2_{P,rms}R_{wp} + I^2_{S,rms}R_{ws}) = 175.4\ W$

Transformer core loss per unit volume $P_v = 3[2(1 + 2^{1-\beta})(D - \frac{1}{6})^{1-\alpha}K_iB^\beta_m f^\alpha_s] = 54.82\ W$

Transformer core loss $P_{Core} = P_vV_e = 54.82x5 = 274.12\ W$

Converter total loss $P_{loss} = P_{C,M} + P_{C,MD} + P_{C,D} + P_{Cu} + P_{Core} = 1210\ W$

Converter efficiency $\eta = \frac{P_o}{P_o+P_{loss}} = 97.64\ \%$.

4.2.8 Total Losses of Three-Phase DC/DC Converter

Fig. 4.6 shows the loss variation of the converter at full load, half load, and 20% of full load condition with $V_o = 420, 350, 250V$. As it can be seen in Fig. 4.6, by increasing the switching frequency, the transformer losses (consist of the copper and core losses) are the main loss and it is around 60% of the total losses. The losses of the body diode of the switches, in same range of the output power for different voltages are constant. By increasing the power level, the average of the output current becomes higher. Therefore, under full load operation, the conduction losses of rectifier diodes are the dominant losses.

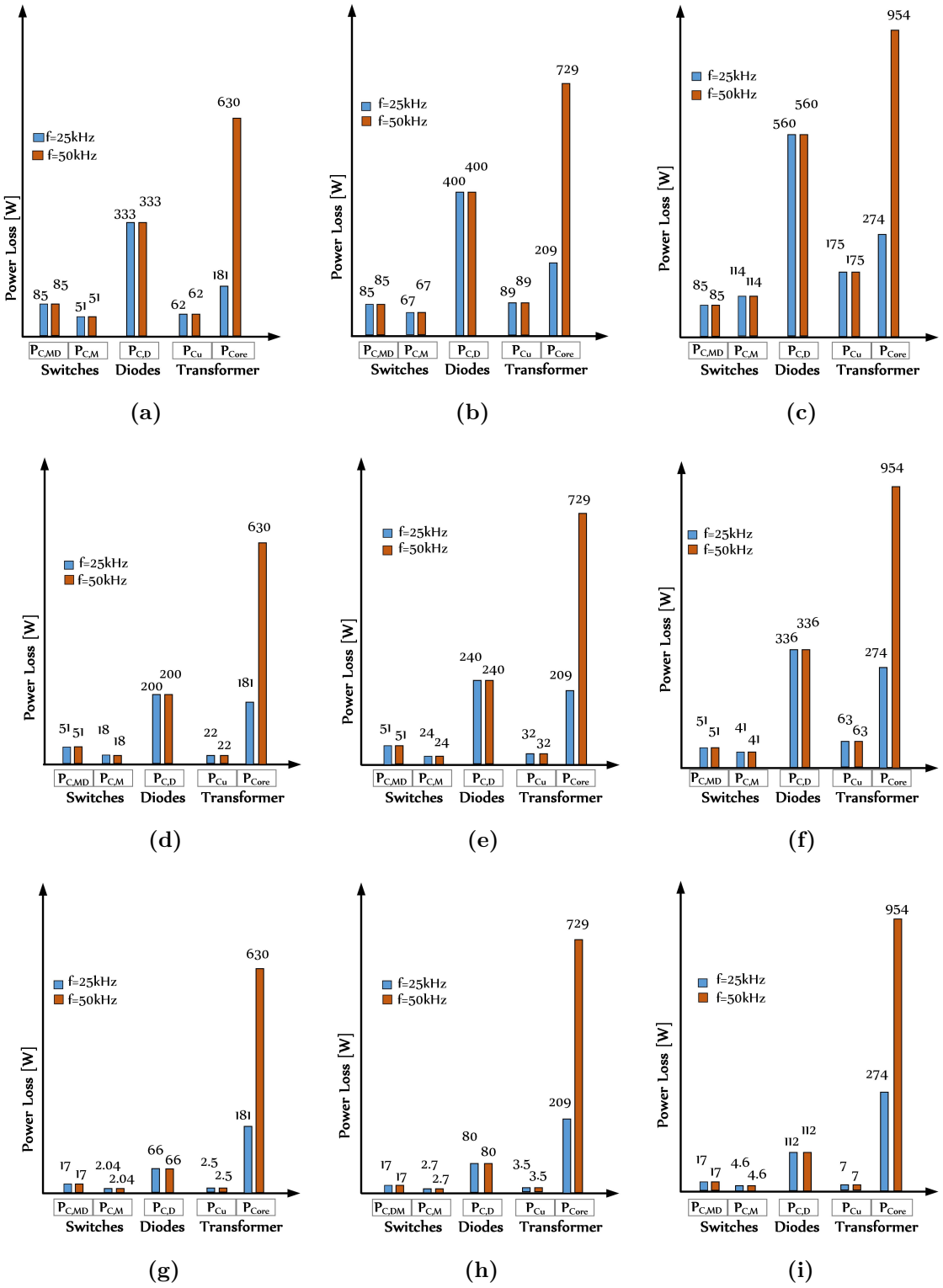

Figure 4.6: Power losses for switches, diodes and transforme
(a) $P_o = 50kW$, $V_o = 420V$ (b) $P_o = 50kW$, $V_o = 350V$ (c) $P_o = 50kW$, $V_o = 250V$
(d) $P_o = 30kW$, $V_o = 420V$ (e) $P_o = 30kW$, $V_o = 350V$ (f) $P_o = 30kW$, $V_o = 250V$
(g) $P_o = 10kW$, $V_o = 420V$ (h) $P_o = 10kW$, $V_o = 350V$ (i) $P_o = 10kW$, $V_o = 250V$

4.2.9 Efficiency of Three-Phase DC/DC Converter

Fig. 4.7 shows the efficiency of the converter for different voltages at $25kHz$ and $50kHz$. As we expected, the efficiency for 25 kHz is higher than $50kHz$, and in $50kHz$ the main losses are related to the transformer.

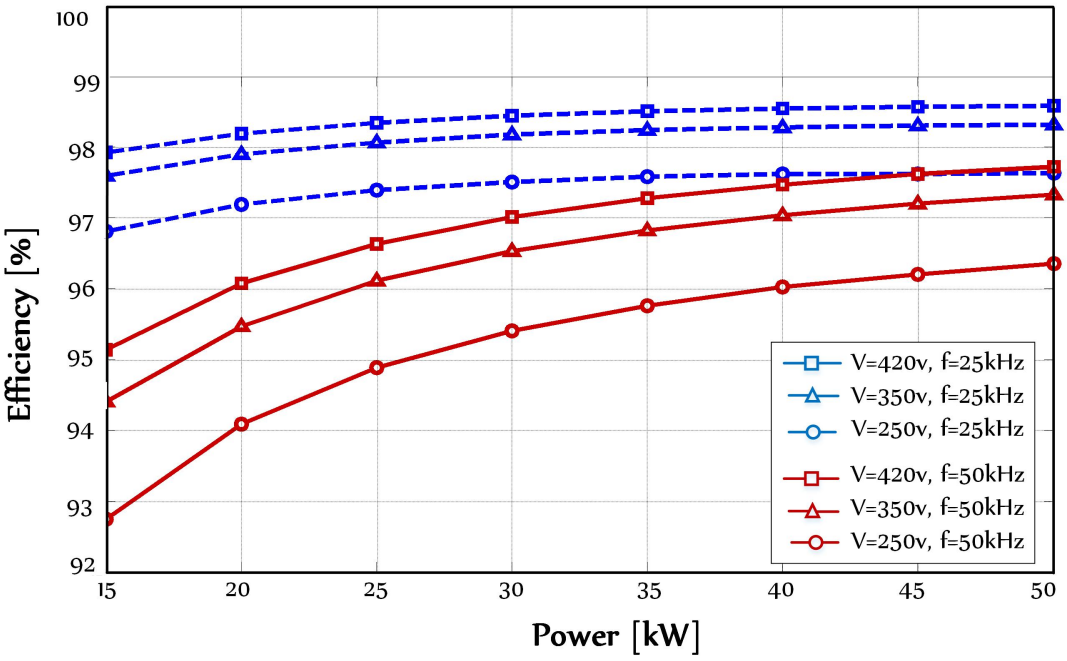

Figure 4.7: Efficiency versus power for $f_s = 25, 50kHz$

As illustrated in Fig. 4.7, total losses become greater, as the switching frequency increases. As a result, the converter's efficiency declines 2% in average for a $50kHz$ switching frequency. On the contrary, the volume of the filters (capacitors, inductors) and transformers becomes smaller and approximately is divided by two. Furthermore, the selection between the two designs depends on the converter goals. If the volume of the converter is an issue, the switching frequency must be selected as much as possible. Otherwise, the switching frequency is chosen 25 kHz so that the losses created by the converter can be reduced.

4.3 Life Cycle Cost Analysis ($LCCA$)

Life cycle cost analysis ($LCCA$) is a process of assessing the economic performance of a specific object over its entire life. This method estimates the total cost of the project, from initial construction through operation and maintenance, and computes the total costs experienced in annual time increments for some span of its life, with consideration of the time value of money. The time value of money, includes a project-specific discount rate, inflation, and cost escalations for different materials and services. $LCCA$ gives an economic model for comparing various design configuration, and evaluates low initial costs and long-term cost savings, and identify the most cost-effective approach among different competing alternatives. [26], [27].

For the application of the fast charger stations, the single-phase and three-phase version of the phase-shift full-bridge converters are investigated in previous sections. As expected, the single-phase PSFB converter has a lower initial cost compared to the three-phase version of this converter but the efficiency of the three-phase one is almost same as the single-phase converter. In the following section, the $LCCA$ method is utilized as a tool to compare these topologies to find out which converter is the more cost-effective system for this application.

4.3.1 Development of $LCCA$ Model

4.3.1.1 Project Cost

In order to develop the $LCCA$ model for the selected topologies in single phase and three phases, it is required to select each component of the converter based on their voltage and current ratings and another considerations as mentioned in the previous sections, and investigate the purchase cost for each item. Initial cost, energy cost, and operation and maintenance are three major costs in the $LCCA$ model [28].

4.3.1.2 Net Present Value

Project costs that occur at various points in the life of a process cannot be compared directly due to the varying time value of money. They must be discounted back to their present value. The results of LCC must be summarized in net present value (NPV) considering the time value of money.

NPV is determined by discounting all project costs to the base, (usually the present year of construction). Thus, the entire project can be expressed as a single base year, or present year cost. Alternatives are then compared by comparing these base year costs [26], [27]. Present value (PV) is the amount of costs at various points in time back to the base year, that can be expressed by

$$PV = \frac{F_V}{(1+r)^n} \tag{4.30}$$

where PV is the present value, F_V is the future value, r is the discount rate, and n

is the number of years of expenditure in the future.

Once all costs and their timing have been developed, future costs are often discounted to the base year and added to the initial cost to determine the NPV for the $LCCA$ alternative. The basic formula is as

$$LCC = C + \sum_{i=1}^{n} PV_i \tag{4.31}$$

where LCC is the life cycle cost, C is the initial cost and PV_i is the present value.

With the net present value calculated for each alternative, comparisons are simple because the units are consistent. The best option is simply the alternative with the lowest life cycle cost or net present value [26], [27].

4.3.2 LCC Model Analysis for $PSFB$ Converter

In this section, the LCC analysis is conducted for the single-phase and three-phase, phase-shift full-bridge converters and determines the optimal candidate system for the fast charger application.

4.3.2.1 Project Cost

This section discusses the selection of the components and materials for the single-phase and three-phase PSFB converters. The presented cost data in Table 4.5 were collected from the respective component manufacturer [5]. According to the topology of these converters the initial cost of them can be calculated easily by adding the cost of their equipment.

1. MOSFET (Half-Bridge Module-1.2KV CAS300Ml2BM2-CREE): 6000 SEK/each module and its driver

2. Rectifier Diode (300 Amp-FRED Modules-600 Volts): 1000 SEK

3. Transformer (Nano-crystalline VITROPERM 500F): 20000 SEK (two toroidal cores (T60004-L2160- W6 6 4-06) stacked together [5])
   The transformer's unit cost comprises the toroidal cores with the winding in the primary and secondary costs.

In this work two topologies of the single-phase and three-phase DC/DC converter have been evaluated for a $50kW$ fast charger station. Based on the calculation in Section 4.1.6, the RMS current for single-phase converter is obtained as $I_{rms} = 169A$ .With the same power and same input/output voltage the RMS current for three-phase converter is calculated as $I_{rms} = 97A$ in Section 4.2.6. It seems that the RMS current in single-phase is $(\sqrt{3})$ times higher than the RMS current in three-phase, which means that in order to have same flux density in the toroidal cores of two topologies it is desired to have $(\sqrt{3})$ times bigger core in the single-phase converter in order to compensate $(\sqrt{3})$ times power losses comparing with the three-phase converter. The same logic is applied for MOSFET selection. Then for the three-phase converter the smaller size of the MOSFET can be used in this topology. The result of the cost for two topologies is depicted in Table 4.5.

Table 4.5: the main components cost data

Component	**Single Phase Converter with 1 single-phase transformers**		**Three Phase Converter with 3 single-phase transformers**	
	Unit	Cost	Unit	Cost
MOSFET and its driver	2	12000	3	10000
Rectifier Diode	4	4000	6	6000
Transformer	1	34000	3	60000
TOTAL COST		50000		76000

-Cost data calculation for the single-phase converter

MOSFET and its driver (Module-1.2KV 300A-CREE)= 6000 $SEKx2 = 12000\ \ SEK$

Rectifier diode (300 Amp-FRED Modules-600 Volts)= 1000 $SEKx4 = 4000\ \ SEK$

Transformer (two toroidal cores stacked together)= 20000 SEK x $\sqrt{3} = 34000\ \ SEK$

-Cost data calculation for the three-phase converter

MOSFET and its driver (Module-1.2KV 200A-CREE)=6000 $SEKx3/\sqrt{3} = 10000$ SEK

Rectifier diode (300 Amp-FRED Modules-600 Volts)= 1000 SEK x 6= 6000 SEK

Transformer (two toroidal cores stacked together)=20000 SEK x 3=60000 SEK

4.3.2.2 Energy Cost

The fast charge stations are charged 2 times per hour and working hours of the stations are 18 hours per day. The charging time is 5 minutes with a power of $200kW$ [29]. The nominal efficiency of these converters is a key to find the cost of energy per year. The energy cost C_P for the PSFB converter can be calculated as

$$C_P = \frac{N}{6}(1-\eta)P_{charge}E_P \tag{4.32}$$

where η is converter's efficiency, N is the working hours of the stations per day, E_P is the electricity price $[2SEK/kWh]$, and P_{charge} is the nominal value of the power transferred to the batteries.

Table 4.6 presents the operation parameter for the single phase and three phase converter with particular components included in the energy cost calculation. The energy costs per year according to (4.32) for the single phase and three phase converters are defined in Table 4.6. It is needed to mention that for this report the operation and maintenance cost are not considered.

Table 4.6: Energy Cost

V_{idc}	700V	Input voltage
V_o	350V	Output voltage
P_{charge}	200kW	Power transferred to the batteries
f_s	25kHz	Switching frequency
η_1	98.80	Efficiency single phase converter
η_3	98.32	Efficiency three phase converter
N	18	Working hours per day
E_P	2 SEK/kWh	Electricity cost
n	10	Number of years in the future
r	0.05	Discount rate
C_{P1}	5256	Energy cost per year for single phase
C_{P3}	7358	Energy cost per year for three phase

4.3.2.3 *LCC* Analysis

Table 4.7 summarizes the *LCC* data used in this analysis.

Table 4.7: The Overview of Life Cycle Cost Analysis

C_{in1}	50000SEK	Initial cost of single phase
C_{in3}	76000SEK	Initial cost of three phase
$PV_{1(1st)}$	5005.7	Present value of single phase for first year
$PV_{3(1st)}$	7008	Present value of three phase for first year
...		
$PV_{1(10th)}$	3226.7	Present value of single phase for year 10th
$PV_{3(10th)}$	4517.4	Present value of three phase for year 10th
LCC_1	90585	Life cycle cost for single phase for 10 years
LCC_3	132820	Life cycle cost for three phase for 10 years

It can be seen from the results in Table 4.7 that the single-phase converter provides a more cost-effective solution in the given $50kW$ power demands for the fast charger. The initial cost and total cost of two alternatives for the *LCCA* model are presented in Fig. 4.8 and Fig. 4.9, respectively.

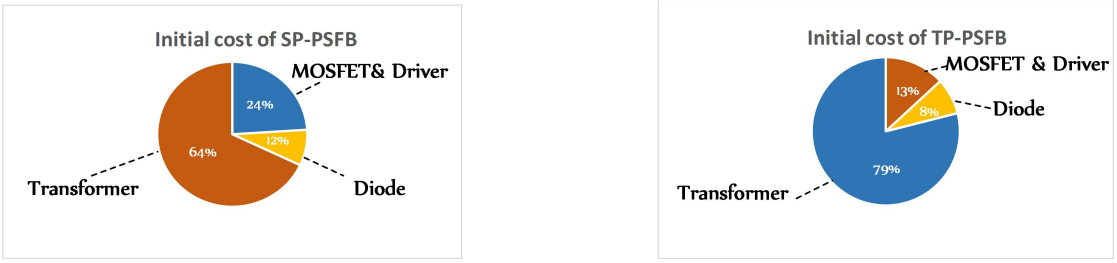

(a) (b)

Figure 4.8: Initial cost of single phase and three phase converter (a) Single phase (b) Three phase

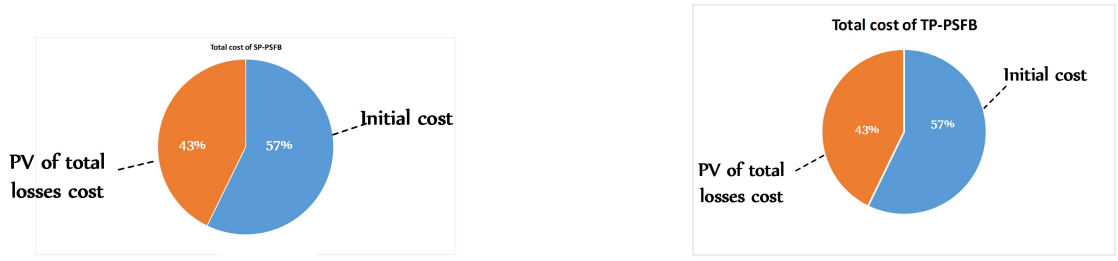

(a) (b)

Figure 4.9: Total cost of single phase and three phase converter (a) Single phase (b) Three phase

4.3.2.4 Pareto Plot

A pareto plot is an effective way to understand the trade-offs between initial cost and value of cost in the future. The pareto plot of life cycle cost is depicted in Fig. 4.10. The initial cost and cost of losses of single-phase and three-phase converters are presented in the form of bars on the vertical axis, and alternative's total life cycle cost is shown by the line. As it is shown, the total life cycle cost of single phase converter is 66% smaller than total life cycle cost of three phase converter.

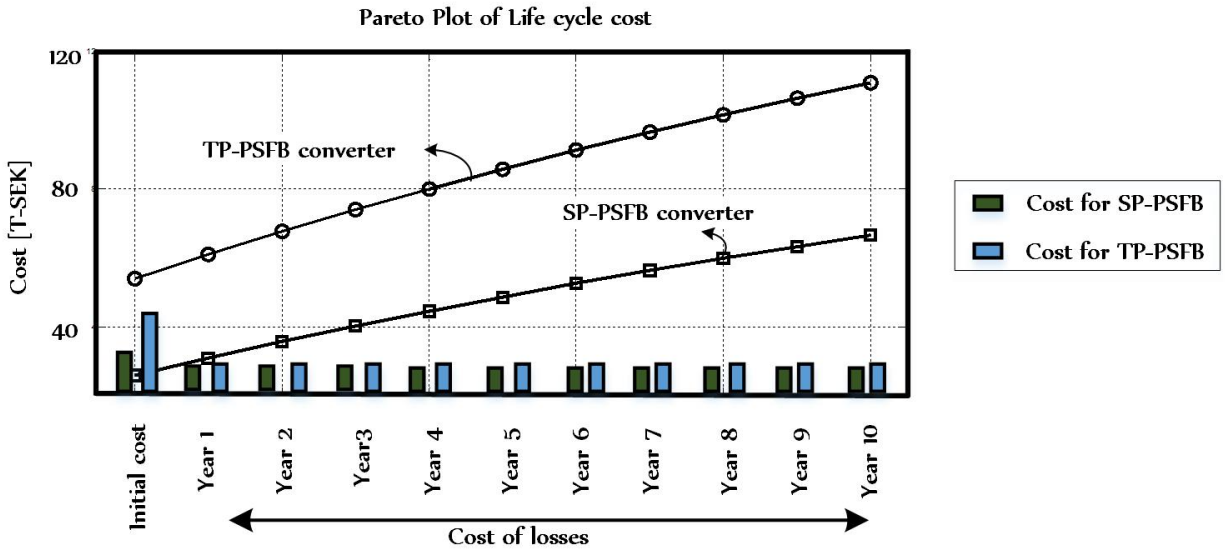

Figure 4.10: Pareto Plot of Life Cycle Cost

4.4 Comparison Between Single-Phase and Three-Phase DC/DC Converter

Table 4.8 shows the components comparison between two topologies. As expected, the number of components in the TP-PSFB are more than the one in the SP-PSFB. The design summary of the two topologies are summarized in Table 4.9. The RMS value of the phase current in the single-phase version is 73% higher than three-phase one. There are two reasons for that the TP-PSFB needs a lower value for the output capacitor; first, the ripple of output current is lower than in the single-phase one; Secondly, the frequency of the output current is three times higher than in single-phase converter.

The different losses of these converters are tabulated in Table 4.10 at $P_{out} = 50\,kW$ and $V_{out} = 250\,V$. The major loss component in this condition for single-phase and three-phase is the conduction loss of the rectifier diode. The total efficiency of the single-phase PSFB is more than for the three-phase PSFB, due to that the core loss of the three-phase one is higher than for the single-phase version. Table 4.11 shows the LCC comparison between these topologies. The LCC of the single-phase is lower than that of the three-phase version. Therefore, it is more cost efficient compared to the three-phase version.

Table 4.8: Topology Comparison for Single and Three-phase DC/DC converter

Parameters	**Single-Phase Converter**	**Three-Phase Converter**
	Unit	Unit
Mosfet switch	4	6
Rectifier diode	4	6
Transformer (two toroidal cores)	1	3
Type of Mosfet switch	1.2KV 300A-CREE	1.2KV 200A-CREE
Type of rectifier diode	300 Amp-600 Volts FRED Modules	300 Amp-600 Volts FRED Modules
Type of transformer	Nano-crystalline VITROPERM 500F	Nano-crystalline VITROPERM 500F

Table 4.9: The design summary of a 50 kW Single and Three-phase DC/DC converter

Parameters		Single-Phase Converter	Three-Phase Converter
Input voltage	V_i	700 V	700 V
Output voltage	V_o	250-420 V	250-420 V
Output power	P_o	50 kW	50 kW
Switching frequency	f_s	25 kHz	25 kHz
Transformer turns ration	n	1.2	1.67
RMS value of phase current	$I_{p,rms}$	169.33 A	97.78 A
Leakage inductance	L_r	1 μH	2 μH
Magnetizing inductance	L_m	600 μH	600 μH
Output inductance	L_f	100 μH	50 μH
Output capacitance	C_o	33 μF	25 μF

Table 4.10: The different losses for Single and Three-phase DC/DC converter

Parameters	Single-Phase Converter	Three-Phase Converter
Input voltage	700 V	700 V
Output voltage	250 V	250 V
Output power	50 kW	50 kW
Switching frequency	25 kHz	25 kHz
Mosfet conduction loss	119.45 W	114.85 W
Mosfet switching loss	0	0
Mosfet, body diode conduction loss	0	85.71 W
Rectifier diode conduction loss	411.42 W	560 W
Transformer copper loss	112.26 W	175.4 W
Transformer core loss	172.82 W	274.12 W
Converter total loss	815.95 W	1210 W
Converter efficiency	98.39 %	97.64 %

Table 4.11: *LCC* summary for Single and Three-phase DC/DC converter

Parameters	Single-Phase Converter	Three-Phase Converter
Initial cost	50000 SEK	76000 SEK
Energy cost per year	5256 SEK	7358 SEK
Present value for first year	5005.7 SEK	7008 SEK
LCC	90585 SEK	132820 SEK

4.5 Results of the Simulation

4.5.1 The Simulation of the Single-Phase Converter

A 50 kW, 700-420 V, 25 kHz prototype is simulated with MATLAB and PLECS Blockset. The waveforms of the Single-Phase Phase-Shifted converter are depicted in Fig. 4.11.

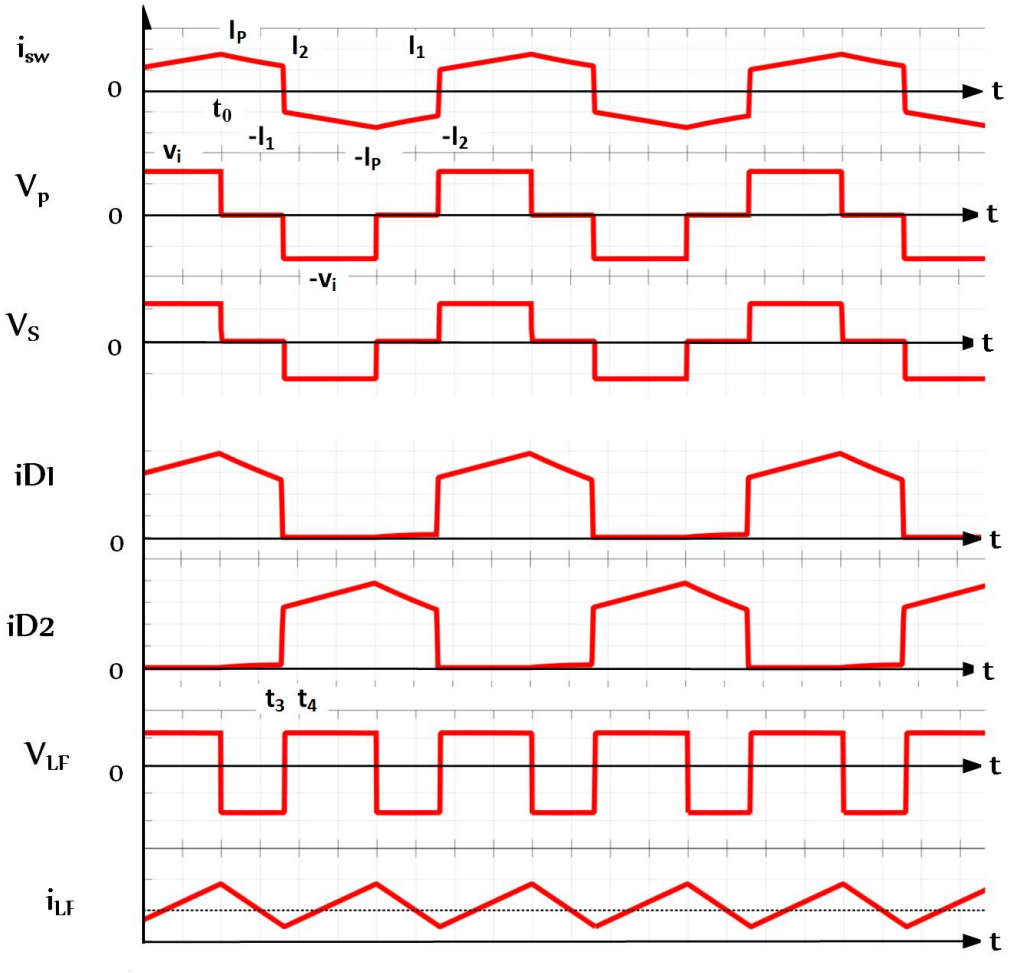

Figure 4.11: The waveforms of the PSFB converter

Fig. 4.12 shows the output voltage and power for different duty cycles. The data has been collected by simulation with the output resistance kept constant with R=3.52 Ω.

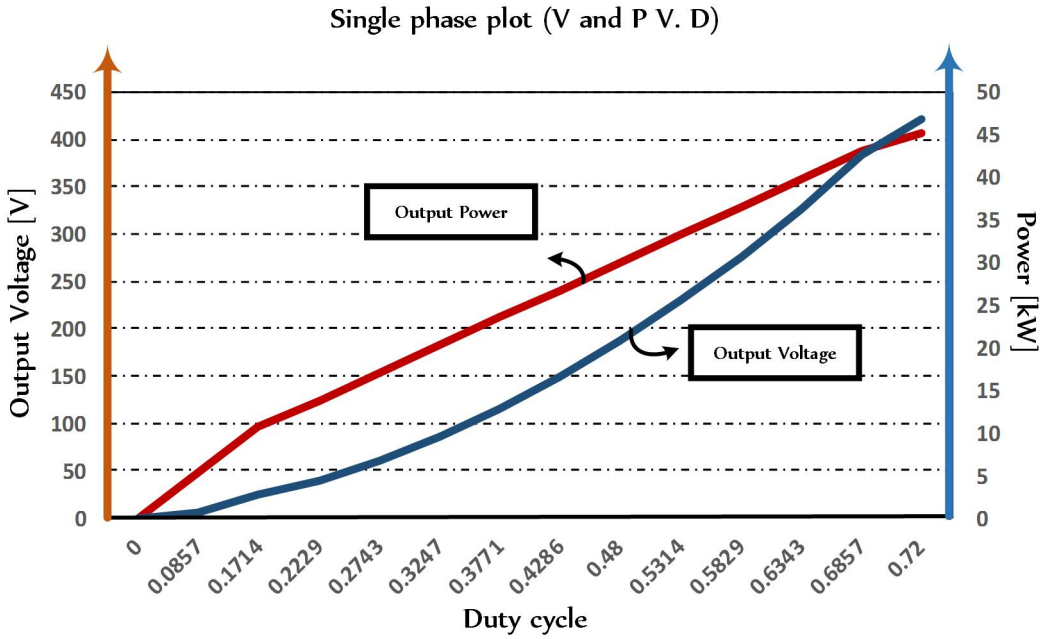

Figure 4.12: The output voltage and power versus duty cycle

4.5.2 The Simulation of the Three-Phase Converter

Fig. 4.13 and Fig. 4.14 show the simulation waveforms of the three-phase converter with a duty cycle of $D = 90°$. The waveforms of the voltage of the transformer phases to the neutral point of input dc source, and the voltage of the transformer phases to the neutral point of the transformer are depicted in Fig. 4.13 and Fig. 4.14 respectively. The characteristics of the converter is as

$V_{idc} = 700V$
$D = 90°$
$f = 25kHz$
$n = n_1/n_2 = 1.67$

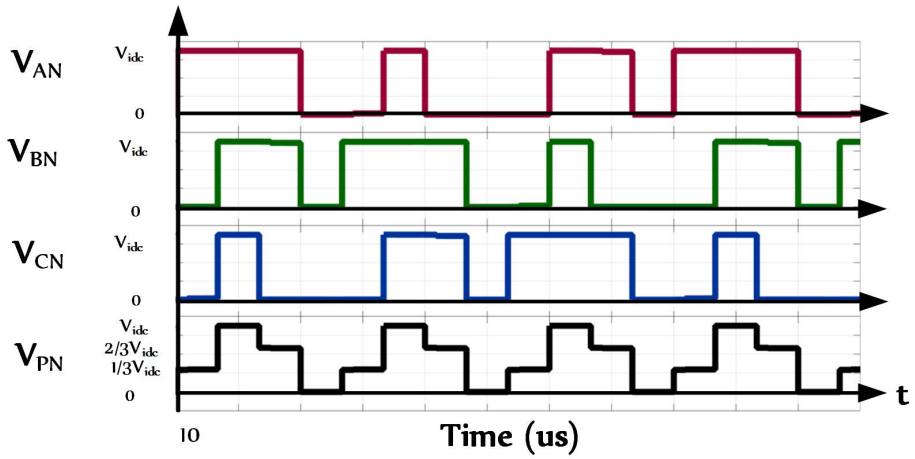

Figure 4.13: Three-phase full-bridge dc-dc converter - Simulation waveforms

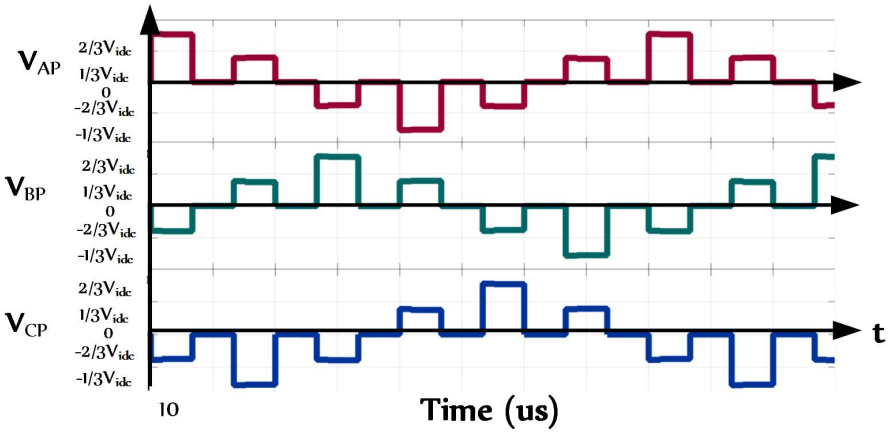

Figure 4.14: Three-phase full-bridge dc-dc converter - Simulation waveforms

The simulation waveforms of the three-phase converter with duty cycle $D = 90°$ and $D = 110°$ are depicted in Fig. 4.15 and Fig. 4.16. The characteristics of the converter is as

$V_{idc} = 700V$
$D = 90°$ and $D = 110°$
$f = 25kHz$
$n = n_1/n_2 = 1.67$

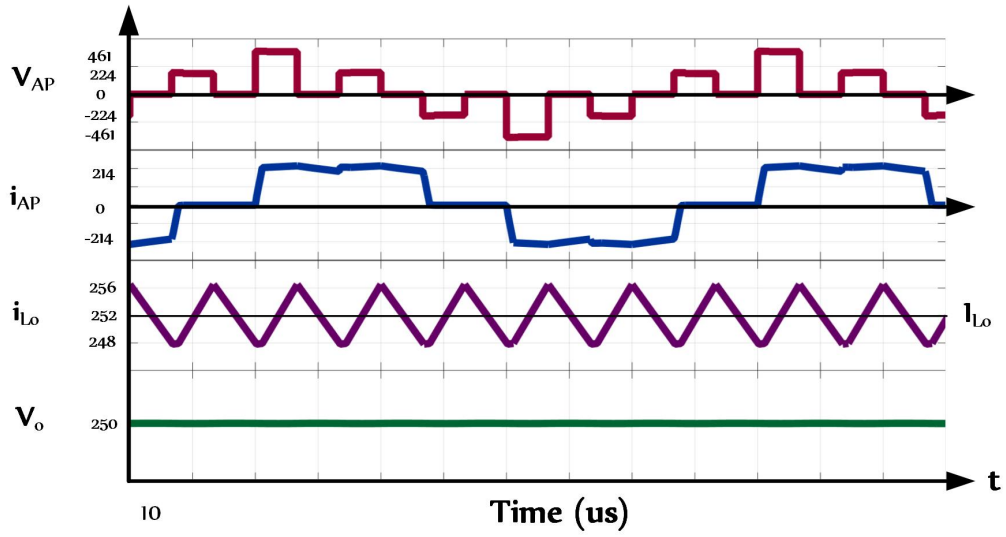

Figure 4.15: Three-phase full-bridge dc-dc converter - Simulation waveforms for $D = 90°$

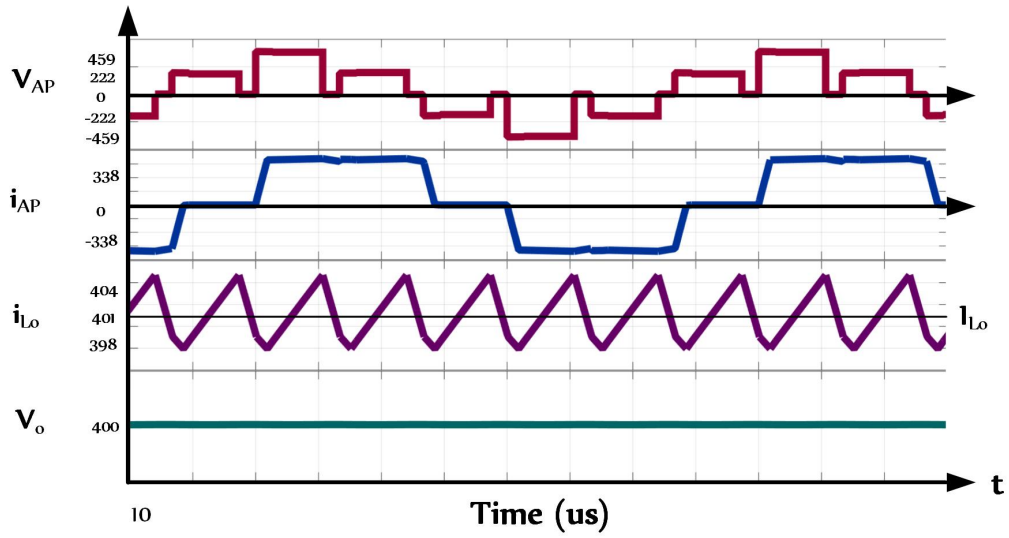

Figure 4.16: Three-phase full-bridge dc-dc converter - Simulation waveforms for $D = 110°$

Fig. 4.17 shows the output voltage and power for different duty cycles. The data has been collected by simulation with the output resistance kept constant with R=3.52 Ω.

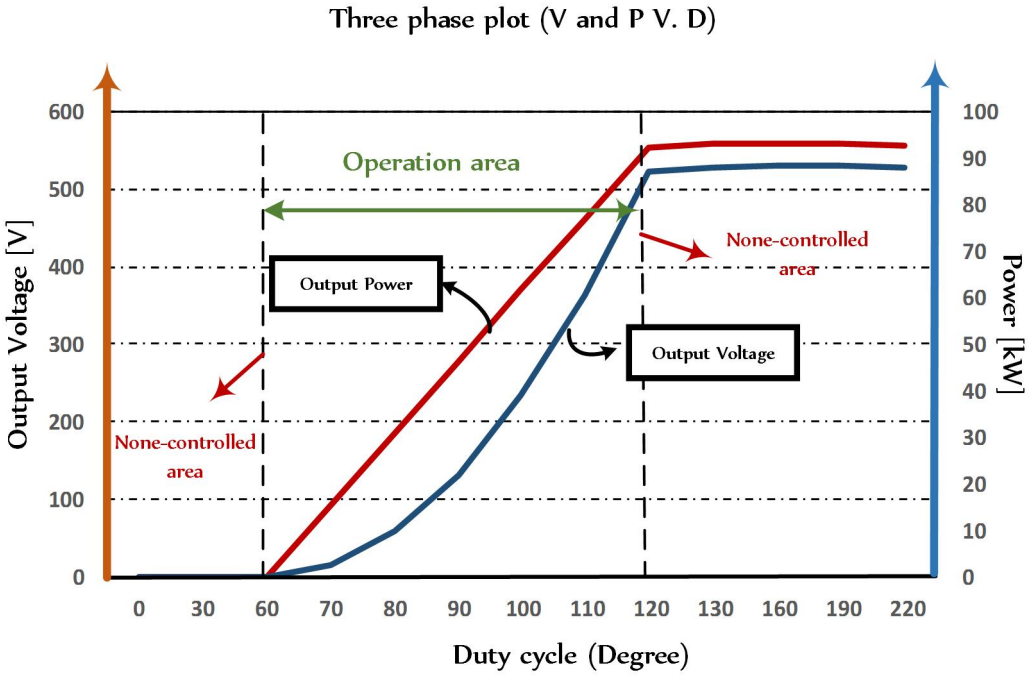

Figure 4.17: The output voltage and power versus duty cycle

5

Conclusion and Future Work

5.1 Results From Present Work

In this work, the power losses for the two topologies of single-phase and three-phase phase-shifted full-bridge converters were analyzed and the efficiency and power losses were calculated for two switching frequencies, and *LCC* analysis was conducted for those two topologies. It was shown that the transformer loss was the dominant loss in those converters, that for 50 kHz switching frequency it was around 60 percent of the total losses. For 25 kHz switching frequency, under full load operation, the conduction losses of the rectifier diodes were the dominant losses.

The overall efficiency of the single-phase converter for 25 kHz was above 99 percent at full load condition and it decreased at light load condition due to the switching losses. The ZVS range for this converter was calculated and it was considered in the power loss analysis. In case of the three-phase converter the overall efficiency at full load condition was about 98.7 percent. The three-phase converter was found to have ZVS condition for the whole range of the output power. A 50 kW 700-420 V 25 kHz prototype was simulated with MATLAB/PLECS Blockset and primary results verified the theoretical analysis.

The *LCC* analysis of the single-phase versus the three-phase version showed that it was more cost efficient compared to the three-phase version. As was discussed in the previous sections, in the three-phase converter, three single core transformers were used. One common three phase core transformer was not available, due to the fact that presently the manufacturing technology has not developed. If one common three phase core is available in the future it seems likely that using one common three phase core transformer in a three-phase circuit will be cost effective and cheaper than three single core transformers.

5.2 Future Work

1. The DC-link capacitor with the rectifier on the DC-side of the converter acts as a storage of DC power and filters out the variations of the DC voltage, and attenuates the ripple currents prior to the converter. A worthy further investigation is to analyze the DC-link current and voltage ripple to find the dimensions of the DC-link capacitor, and evaluate converters with DC-link capacitors in terms of their losses, efficiencies and costs.

2. In this thesis, a high frequency transformer with $Y-Y$ windings in the three-phase DC/DC converter is selected. Regardless of the magnetic construction, different transformer-winding configurations, such as $Y-\Delta$ and the $\Delta-\Delta$ can be utilized in a three-phase DC/DC converter. A comparison between different transformer-winding configurations, and their impact on the performance of the three-phase DC/DC converter can be an interesting research topic in the future.

3. Furthermore, design optimization of a power transformer including core shapes, different core materials, and thermal models can be carried out. In case of a three-phase transformer, different shapes of the core consisting of three-legs, four-legs, and five-legs with a common core can be investigated and the influence of operation and cost on the three-phase DC/DC converter can be evaluated.

Bibliography

[1] J. C. G. Justino, T. M. Parreiras and B. J. Cardoso Filho, "Hundreds kW Charging Stations for e-Buses Operating Under Regular Ultra-Fast Charging," in *IEEE Transactions on Industry Applications*, vol. 52, no. 2, pp. 1766-1774, March-April 2016.

[2] F.Yazdani, S. Haghbin, T. Thiringer, M. R. Zolghadri, "Analysis of a Three-Phase Dual Active Bridge Converter During the Deadband" in *2017 IEEE International Conference on Environment and Electrical Engineering and 2017 IEEE Industrial and Commercial Power Systems Europe (EEEIC / ICPS Europe)*, Milan, 2017.

[3] Thiringer, T.; Haghbin, S. Power Quality Issues of a Battery Fast Charging Station for a Fully-Electric Public Transport System in Gothenburg City. Batteries 201 5, I, 22-33.

[4] M. Yilmaz and P. T. Krein, "Review of Battery Charger Topologies, Charging Power Levels, and Infrastructure for Plug-In Electric and Hybrid Vehicles," in *IEEE Transactions on Power Electronics*, vol. 28, no. 5, pp. 2151-2169, May 2013.

[5] S. Haghbin, "Design considerations of a 50 kW compact fast charger stations using nanocrystalline magnetic materials and SiC modules," *2016 Eleventh International Conference on Ecological Vehicles and Renewable Energies (EVER), Monte Carlo*, 2016, pp. 1-6.

[6] Tai-Ran Hsu. On the Sustainability of Electrical Vehicles. November 2013.San Jose State University,CA 95192-0087.

[7] IEEE.org. *"IEEE Code of Ethics"*, 2016. [Online]. Available:`http://www.ieee.org/about/corporate/governance/p7-8.html/`

[8] Hongmei Wan, " High Efficiency DC-DC Converter for EV Battery Charger Using Hybrid Resonant and PWM Technique", *Master thesis submitted to the faculty of the Virginia Polytechnic Institute*, Blacksburg, Virginia, April 30, 2012.

[9] Changrong Liu, " A Novel High-Power High-Efficiency Three-Phase Phase-Shift DC/DC Converter for Fuel Cell Applications", *Phd dissertation submitted to the faculty of the Virginia Polytechnic Institute*, Blacksburg, Virginia, January 25, 2005.

[10] Jialong Wang and Raluca Lascu, "Zero sequence circuit of three-legged core type transformers," *2009 62nd Annual Conference for Protective Relay Engineers*, Austin, TX, 2009, pp. 188-213.

[11] Jing Xue, "Single-phase vs. Three-phase High Power High Frequency Transformers", *Thesis submitted to the Faculty of the Virginia Polytechnic Institute*,Blacksburg, VA, April 29, 2010.

[12] Mattias Persson and Waqas Baig, "Modeling and Measurements of Transformer Behavior at Different Voltages and Frequencies", *Master thesis submitted to the CHALMERS UNIVERSITY OF TECHNOLOGY*, Göteborg, Sweden, 2011.

[13] JP Transformer Book 12th edition, 1998, ISBN 07506 1158 8.

[14] E. Agheb, M. A. Bahmani, H. K. Høidalen, and T. Thiringer, "Core loss behavior in high frequency high power transformers—II: Arbitrary excitation," *Journal of Renewable and Sustainable Energy* 4, vol.4, Issue:3, pp: 033113 June 2012.

[15] S. Haghbin and T. Thiringer, "3.3kW Onboard Battery Chargers for Plug-in Vehicles: Specifications, Topologies and a Practical Example," *International Journal of Electronics and Electrical Engineering*, vol. 4, No. 1, February 2016.

[16] J. A. Sabate, V. Vlatkovic, R. B. Ridley, F. C. Lee, and B. H. Cho, "Design considerations for high-voltage high-power full-bridge zero-voltage-switched PWM converter," in *Applied Power Electronics Conference and Exposition*, 1990. APEC '90, Conference Proceedings 1990., Fifth Annual, March 1990, pp. 275-284.

[17] A. Mallik, and A. Khaligh," Variable-Switching-Frequency State-Feedback Control of a Phase-Shifted Full-Bridge DC/DC Converter," in *IEEE Transactions on Power Electronics*, vol. 32, no. 8, August 2017.

[18] Y. Jang and M. M. Jovanovic, "A new PWM ZVS full-bridge converter," *IEEE Trans. Power Electron.*, vol. 22, no. 3, pp. 987–994, May 2007.

[19] W. L. Weeks, Transmission and Distribution of Electrical Energy (Harper Row, 1981), p. 38.

[20] F. E. Terman, Radio Engineers' Handbook, (McGraw-Hill, 1943), p. 37.

[21] Yuancheng Ren, Ming Xu, Jinghai Zhou and F. C. Lee, "Analytical loss model of power MOSFET," in *IEEE Transactions on Power Electronics*, vol. 21, no. 2, pp. 310-319, March 2006.

[22] A. R. Prasad, P. D. Ziogas and S. Manias, "Analysis and design of a three-phase offline DC-DC converter with high-frequency isolation," in *IEEE Transactions on Industry Applications*, vol. 28, no. 4, pp. 824-832, Jul/Aug 1992.

[23] L. Gu, K. Jin and C. Liu, "Current-tripler-rectifier pulse width modulation ZVS three-phase full-bridge DC/DC converter with Y– connected transformer," in *IET Power Electronics*, vol. 8, no. 7, pp. 1111-1118, 7 2015.

[24] N. Mohan, T. Undeland, and W. Robbins, Power electronics converters, applications, and design. Wiley, 2 edition, 1995.

[25] `https://en.wikipedia.org/wiki/American_wire_gauge`

[26] P. E. H. Paul Barringer, "A life cycle cost summary," in *Proc. Int. Conf. Maintenance Soc. (ICOMS)*, 2003, pp. 1–10.

[27] Environmental Stewardship Committee, Stanford University, Guidelines for Life Cycle Cost Analysis, October 2005.

[28] H. Li, L. Qu and W. Qiao, "Life-cycle cost analysis for wind power converters," *2017 IEEE International Conference on Electro Information Technology (EIT), Lincoln, NE*, 2017, pp. 630-634.

[29] Thiringer, T.; Haghbin, S. Power Quality Issues of a Battery Fast Charging Station for a Fully-Electric Public Transport System in Gothenburg City. *Batteries* 2015, 1, 22-33.

A

Appendix 1

A.1 Paper

Design Of a 50 kW Phase-Shifted Full-Bridge Converter Used For Fast Charging Applications

Nadia Hassanzadeh
Electric Power Engineering Division
Chalmers University of Technology
hnadia@student.chalmers.se

Farzad Yazdani
Electric Power Engineering Division
Chalmers University of Technology
Yazdani_farzad@ee.sharif.edu

Saeid Haghbin
Electric Power Engineering Division
Chalmers University of Technology
saeid.haghbin@chalmers.se

Torbjorn Thiringer
Electric Power Engineering Division
Chalmers University of Technology
torbjorn.thiringer@chalmers.se

***Abstract*— A phase-shift full-bridge (PSFB) converter with MOSFET switches is widely used for the dc/dc stage of high power applications such as energy storage systems. The significant advantage of the PSFB converter compared to a dual active bridge converter is its reduced cost due to utilizing the diode rectifiers instead of active switches in the secondary side of the converter. However, operating in zero voltage switching (ZVS) is important to achieve higher level of efficiencies. Hence, a higher switching frequency operation with a higher power density can be obtained. In this paper, the design of the PSFB dc/dc converter based on theoretical calculations is presented; the different losses in the converter are discussed.**

Keywords—DC/DC converter; full-bridge; ZVS; phase-shift; fast charger;

I. INTRODUCTION

The needed time for charging is one of the challenges for EVs as an alternative to internal combustion engines (ICE vehicles). A problem with currently available DC fast chargers is low-frequency switching which increases the size, weight, and cost of many fast chargers. Nowadays, there are some experiments of fast chargers for urban electrical buses like the electrical buses in Santa Barbara, U.S., and electrical buses recently presented in Geneva, Switzerland [1-2]. One of the bus charger stations in Sweden with a 300 kW power level is shown in Fig. 1. Common trends for charger are the movement towards smaller size and more efficient stations while the cost is reduced [3].

One of the most common dc/dc converter topologies in the medium and high-power applications is a phase-shifted full bridge (PSFB) converters as depicted in fig. 2 [4]. Considerable advantages of the PSFB converter compared to the classical hard switched converter is its high efficiency, high power density, high reliability, and low EMI due to ZVS operation [5]. The output power of the PSFB varies with a phase shift between the duty cycles of any two diagonally switches in the left leg and the right leg of the primary side of the converter [6].

With the phase shift of zero, the duty cycle will be 1 which results in hard-switched operation of the converter. In the case that the phase-shift angle equals 180 degrees, the duty cycle will be zero and there is no power transfer [4].

Fig. 1. A fast charging bus station with a 300 kW charger unit in Sweden

The achievement of the high efficiency of power conversion needs to ensure ZVS operation at the light-load condition. This is a design challenge which is suggested to consider up to 50% of the nominal load [4]. To evaluate the efficiency of a PSFB an accurate loss analysis of the converter is necessary which takes into account the evaluation of switching and conduction losses of switches, conduction losses of the rectifier, the magnetic and winding losses of the transformer. The purpose of this paper is to evaluate the power losses and efficiency of a sample design of the PSFB as a function of the switching frequency. The range of the ZVS operation to achieve high conversion efficiency is discussed. Various losses in the circuit related to the power switches and the transformer are defined. The simulation results of a 50kW PSFB verify the theoretical analysis.

II. PHASE-SHIFT FULL-BRIDGE DC/DC CONVERTER

Fig. 2 shows a phase-shift full-bridge (PSFB) dc/dc converter [4]. The converter specification for the design of the 50 kW system is presented in table I. It is suggested to utilize 1.2 kV SiC MOSFET switches in the converter to get low switching losses. The MOSFET output capacitor (C_{oss}) of the SiC switch is 2.5 nF according to the datasheet. A metallic tape-wound core made of the nanocrystalline VITROPERM 500 F is used for the isolated transformer. The resulting

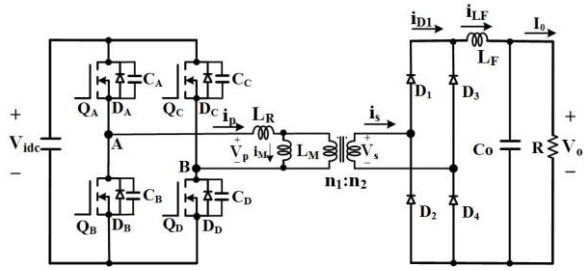

Fig. 2. Single-phase PSFB DC/DC converter

TABLE I
SPECIFICATION OF THE PSFB CONVERTER

arameter	Symbol	Value
Input voltage	V_{idc}	$700\ V$
Output voltage	V_o	$250 - 420\ V$
Nominal Power	P_T	$50\ kW$
Switching frequency	f_s	$25\ kHz$

TABLE II
DESIGNED PARAMETERS

Parameter	Symbol	Value
Output capacitor of FET	C_{oss}	$2.5\ nF$
Leakage inductor	L_R	$1\ \mu H$
Magnetizing inductor	L_M	$600\ \mu H$
Output filter	L_F	$100\ \mu H$
Output capacitor	C_O	$33\ \mu F$

transformer capacitance is ignored in this work. The design procedure is presented in the following section. The designed parameters are shown in table II.

A. Resonance circuit calculation

For achieving ZVS operation, the energy stored in the leakage inductance must be more than the energy needed for charging and discharging of the output capacitors of the switches during the dead time [7]. The required energy in the resonance inductance L_R is

$$E = \frac{1}{2}L_R I_2^2 > \frac{4}{3}C_{oss}V_{idc}^2 + \frac{1}{2}C_T V_{idc}^2 \quad (1)$$

where L_R is the transformer leakage inductance, C_{oss} is the switch output capacitance, C_T is the transformer winding capacitance, I_2 is the primary current of the transformer at the left leg or the right leg transition time and V_{idc} is the input voltage.

The critical current in the primary of the transformer for the ZVS operation is as

$$I_{crit} = \sqrt{\frac{C_R V_{idc}^2}{L_R}} \quad (2)$$

where $C_R = \frac{8}{3}C_{oss} + C_T$.

ZVS is achieved for the condition where the primary current of the transformer (I_2) at the transition time is higher than the critical current [7].

The second condition for ZVS operation is enough dead time for the transition between switches in each leg to ensure that the output capacitor of each switch discharges completely. However, with a long dead time, the output capacitor of the switch will discharge and continue to resonate and then drop. The resonance between L_R, C_{oss}, and C_T provides a sinusoidal voltage across the switch capacitance which reaches its peak value at one fourth of the resonance period, that can be expressed as [7]

$$T_{max} = \frac{T}{4} = \frac{\pi}{2}\sqrt{L_R C_R}. \quad (3)$$

B. Design procedure

A metallic tape-wound core made of the nanocrystalline VITROPERM 500 F is used for the isolated transformer which gives very low transformer capacitance (C_T), near zero. By applying D_{min} and D_{max} the required transformer turn's ratio is obtained as $n = 1.2$ which gives a maximum duty cycle of around $D = 0.72$.

$$D_{min} = \frac{nV_{o,min}}{V_{in}} \quad (4)$$

$$D_{max} = \frac{nV_{o,max}}{V_{in}}$$

Here $V_{o,min}$ and $V_{o,max}$ are the minimum and maximum output voltage which is equal 250 and 420 respectively. The transformer turns-ratio (n) is the number of the turns of the winding in the primary over the secondary. In order to calculate the minimum value of the leakage inductance, it is required to consider 50% of the full load. For this reason, the minimum value of the leakage inductance can be calculated as follow [4]

$$L_R = \frac{2E}{i_L^2} = 1\mu H \quad (5)$$

Here E is the leakage inductance energy which can be achieved by employing (1).

By considering $\Delta I_o = 0.1 I_o$ the needed magnetization inductance of the transformer can be calculated as [4]

$$L_M \geq \frac{nDV_{in}}{4\Delta I_o f_s} = 600\mu H. \quad (6)$$

Then, the minimum output inductor value is expressed as [4]

$$L_f \geq \frac{V_{o,nom}(1 - D_{nom})}{4\Delta I_o f_s} = 100\mu H. \quad (7)$$

If the output voltage ripple is supposed to be less than $1V$ ($\Delta Vo \leq 1V$), then, the output capacitor is defined as [4]

$$C_o \geq \frac{\Delta I_o T_s}{16 \Delta V_o} = 33\mu F. \quad (8)$$

C. Zero voltage switching range

Fig. 3 shows the transformer primary current. At right leg transition (time between t_0 and t_1), the primary current of the transformer has its peak value, which is the reflected current of the secondary of the transformer with the highest current through the output filter. Then the ZVS can be achieved for the right leg transistors easily even at the light loads [7].

The ZVS of the left leg of the converter is achieved for the condition when the stored energy of the leakage inductance is available enough to charge and discharge the output capacitances. At the left leg transition (time between t_2 and t_3) in the secondary side of the converter all diodes are conducting and there is a short circuit across the secondary side of the transformer. Then the primary current of the transformer is i_{t2} with a value lower than the peak current. In this case for the light loads, the ZVS will be lost. With high input voltage which requires more capacitive energy, the condition is worse [7].

Fig. 4a shows the waveforms of the converter at as input voltage equal to 350V , $f_s =$ 25kHz, and as output power equal to $P_o = 23$ kW. As can be seen from the figure, at this range of output power the output capacitors of the switches don't have enough time to charge and discharge during the dead time, then ZVS operation is lost, which is predicted by analysis when the load current is below the critical current in (2). In Fig. 4b ZVS operation is achieved in the mentioned condition for the output power equal to $P_o = 27\ kW$.

By using I_{crit} and I_2 , P_{ZVS} for the boundary conditions of ZVS operation is founded. It is indicated that by increasing the frequency, if $\Delta Io > I_M$, P_{ZVS} increases, and if $\Delta Io < I_M$, P_{ZVS} decreases. In our proposed design, $\Delta Io < I_M$ then, by increasing the frequency, the power boundary gets wider region for ZVS operation.

$$I_{crit} = \sqrt{\frac{C_R V_{idc}^2}{L_R}} \quad (9)$$

$$I_2 = I_M + \frac{I_o - \Delta I_o}{n} \quad (10)$$

$$P_{ZVS} = V_o[n(I_P - I_M) + \Delta I_o] \quad (11)$$

Fig. 5 shows ZVS operation region for three frequencies versus different output voltages for different output powers. As

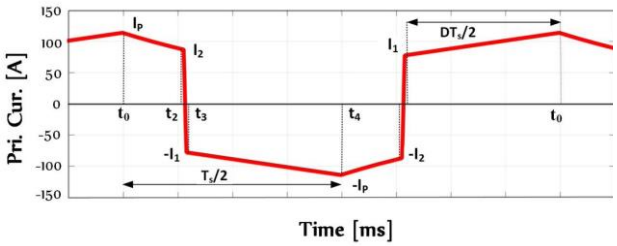

Fig. 3. The transformer primary current

it is shown for $f_s = 100kHz$, the ZVS region is wider than $f_s = 25kHz$, but the drawback in this case is that by increasing

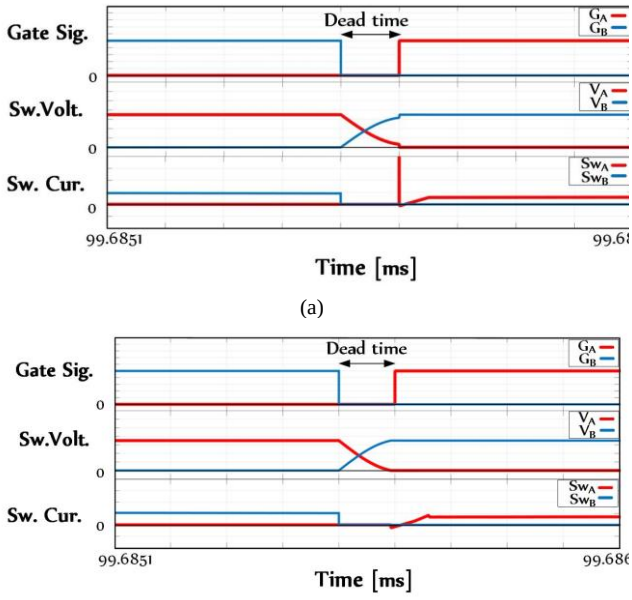

Fig. 4. The gating signals, voltage and current waveforms of left leg switches (a) without ZVS operation (b) with ZVS operation

the switching frequency, switching losses increases, and

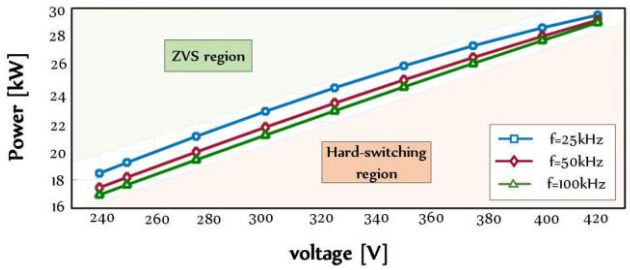

Fig.5. ZVS boundaries for three different frequencies

therefore the efficiency decreases.

III. Phase-Shift Full-Bridge DC/DC Converter

In order to optimize the efficiency of the PSFB converter, it is necessary to calculate the power losses accurately. In this section, different losses of this converter are determined as a function of the switching frequency. The power losses in each switch-mode converter are switching losses and conduction losses of semiconductors, copper losses and core losses of the transformer.

A. Switching losses

Due to the overlapping between voltage and current of the switch during switching transition, switching loss is generated. Since the PSFB is operating in ZVS condition, the switching loss can be neglected. Although, for non-ZVS condition, the switching loss can be calculated as [8]

$$P_{sw} = \frac{1}{2}(V_{sw}I_{sw})(t_f + t_r)f_{sw} + \frac{1}{2}C_{ds}V_{sw}^2 f_{sw} \quad (12)$$

where V_{sw} and I_{sw} are the voltage and current of the switch in the instance of the transition, t_f and t_r are the falling and rising time of the switch, and C_{ds} is the drain-source capacitor of the switch.

B. Conduction loss

The switch and diode conduction losses are obtained by using the following equations [4]

$$P_{C,M} = 4R_{DS}(on)I_{Mos,rms}^2 \quad (13)$$

$$P_{C,D} = 4I_D V_D \quad (14)$$

where $R_{DS}(on)$ is the drain-source resistor of the switch, $I_{Mos,rms}$ is RMS value of the switch current, V_D is the turn-on voltage of the diode, and I_D is the averaged value of the diode's current.

C. Copper loss

The copper losses for both transformer sides can be calculated as [9]

$$P_{Cu} = I_{p,rms}^2 R_{wp} + I_{s,rms}^2 R_{ws} \quad (15)$$

where $I_{p,rms}$ and $I_{s,rms}$ are the RMS value of the currents of the primary and secondary side of the transformer, and R_{wp} and R_{ws} are the resistors of the primary and secondary winding.

D. Core loss

An empirical Steinmetz Equation is generally used for core loss calculation of the transformer, but it does not give accurate answers under non sinusoidal excitation, since the equation depends only on the peak value of the magnetic induction. The improved general Steinmetz equation (IGSE) is one of the most accurate methods for core loss calculation, which extends Steinmetz Equation for non-sinusoidal waveforms. According to IGSE the transformer core loss per unit volume is expressed as [10]

$$p_{Core} = 2^{\beta+\alpha} D^{1-\alpha} K_i f^{\alpha} B_m^{\beta} \quad (16)$$

and transformer core loss is given by

$$P_{Core} = p_{Core} V_e \quad (17)$$

where B is the maximum flux density, $K_i, \alpha \; and \; \beta$ are the core material constants, D is the duty cycle of the signals, and V_e is the total volume of the core.

Total losses are the sum of losses of switches (conduction and switching loss), diodes (conduction loss) and transformer (core and copper losses). Therefore, the efficiency of the converter is expressed as

$$P_{Loss} = P_{C,M} + P_{SW} + P_{C,D} + P_{CU} + P_{Core} \quad (18)$$

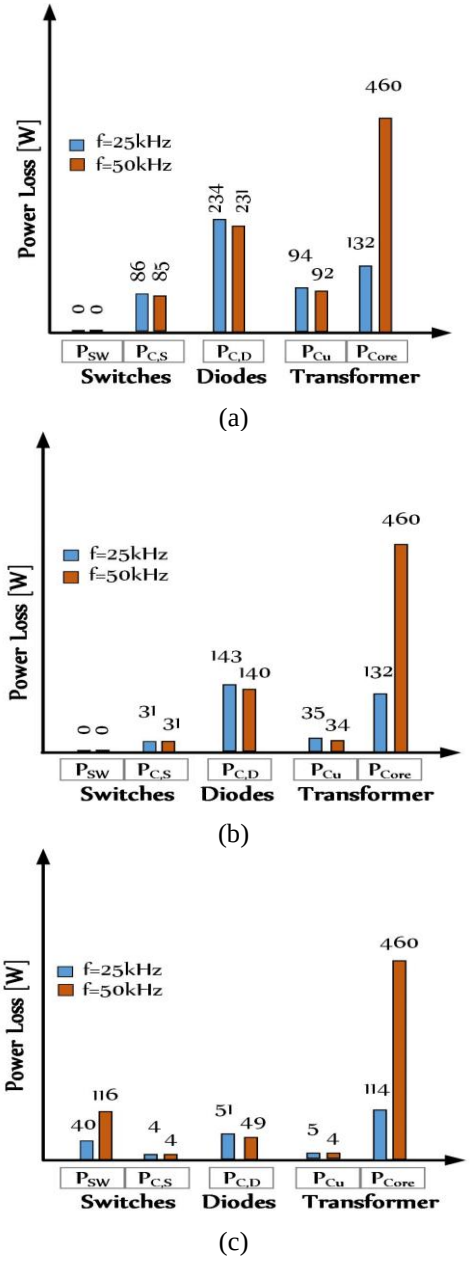

Fig. 6. Power losses for switches, diodes and transformer
(a) Po = 50kW, Vo = 350V (b) Po = 30kW, Vo = 350V
(c) Po = 10kW, Vo = 350V

$$\eta = \frac{P_o}{P_o + P_{loss}}. \quad (19)$$

According to (16), the core loss of the transformer depends on switching frequency and duty cycle of the excitation voltage waveform. For $V_{out} = 250V$ the duty cycle has its minimum value, or $D^{1-\alpha}$ is maximum. Therefore, the maximum core loss occurs in this case. The amount of core loss is constant in whole range of output power. By increasing the power level, the RMS

value of leakage inductors current becomes higher. Therefore, under full load operation, conduction and copper losses are the dominant losses. Fig. 6 shows the loss variation of the converter at full load, half load, and 20% of full load condition with $V_o = 350V$. As it can be seen in Fig. 6, at a higher switching frequency, the transformer losses (consist of the copper and core losses) are the main loss and it is around 60% of the total losses.

IV. Simulation Results

The main parameters of the PSFB converter are shown in Table I. The input voltage is regulated and its value is $700\ V$, the storage battery is connected to port 2 and its voltage is varied between $250\ V$ to $420\ V$. The leakage inductance of the transformer is $1\ \mu H$. The switches in the input are half-bridge SiC modules from CREE, type CAS300M12BM2. The output capacitor (C_{oss}) of the SiC switch is $2.5\ nF$ according to the datasheet. Fig. 7 shows the efficiency of the converter for different voltages at $25\ kHz$ and $50\ kHz$. In $50\ kHz$ the main losses are related to the transformer. As shown in Fig.7, the efficiency at full load condition are 99% and 97.5 for $f_{sw} = 25\ kHz$ and $f_{sw} = 50\ kHz$, respectively. For light load condition, the efficiency is reduced because of the increase of the switching loss. The waveforms of the PSFB converter are depicted in Fig. 8.

V. Conclusions

In this paper, the power losses of the PSFB are analyzed and the efficiency and power loss are calculated for two switching frequencies. It is shown that the transformer loss is the dominant loss in this converter for $50\ kHz$ switching frequency where it is around 60 percent of the total losses. The overall efficiency of this converter for $25\ kHz$ is above the 99 percent at full load condition and it decreases at light load condition due to the switching losses. The ZVS range for this converter is calculated and it is considered in the power loss analysis. A $50\ kw$ $700 - 420\ V$ $25\ kHz$ prototype is simulated and primary results verify the theoretical analysis.

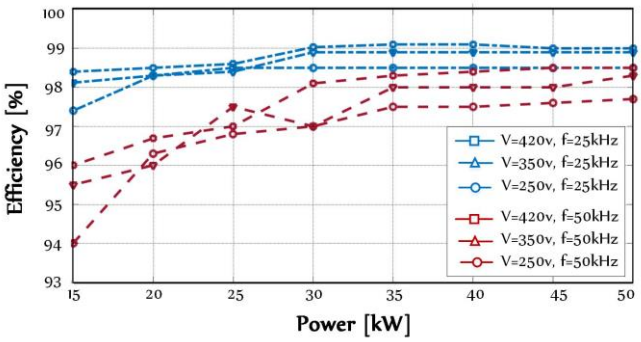

Figure 7. Efficiency versus power for $f_s = 25, 50kHz$

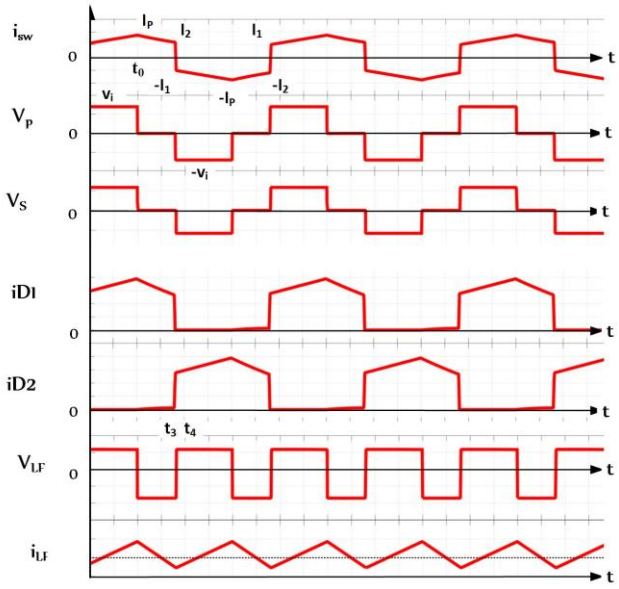

Figure 8. The waveforms of the PSFB converter

Acknowledgment

The authors would like to thank Swedish Energy Agency for the project financing and VACUUMSCHMELZE for providing transformers

References

[1] J. C. G. Justino, T. M. Parreiras, and B. J. C. Filho,"Charging Stations for e-Buses Operating Under Regular Ultra-Fast Charging," in *IEEE Transactions on Industry Applications*, vol. 52, no. 2, March/April 2016.

[2] Opbrid Bus Bar, Granada, Spain. [Online]. Available: www.opbrid.com.

[3] F.Yazdani, S. Haghbin, T. Thiringer, M. R. Zolghadri, "Analysis of a Three-Phase Dual Active Bridge Converter During the Deadband" in 2017 IEEE International Conference on Environment and Electrical Engineering and 2017 IEEE Industrial and Commercial Power Systems Europe (EEEIC / I&CPS Europe), Milan, 2017.

[4] S. Haghbin and T. Thiringer, "3.3kW Onboard Battery Chargers for Plug-in Vehicles: Specifications, Topologies and a Practical Example," *International Journal of Electronics and Electrical Engineering*, vol. 4, No. 1, February 2016.

[5] P. K. Jain, W. Kang, H. Soin, and Y. Xi, "Analysis and design considerationsof a load and line independent zero voltage switching full bridge DC/DC converter topology," IEEE Trans. Power Electron., vol.17, no. 5, pp. 649–657, Sep. 2002.

[6] A. Mallik, and A. Khaligh," Variable-Switching-Frequency State-Feedback Control of a Phase-Shifted Full-Bridge DC/DC Converter," in *IEEE Transactions on Power Electronics*, vol. 32, no. 8, August 2017.

[7] J. A. Sabate, V. Vlatkovic, R. B. Ridley, F. C. Lee, and B. H. Cho, "Design considerations for high-voltage high-power full-bridge zero-voltage-switched PWM converter," in Applied Power Electronics Conference and Exposition, 1990. APEC '90, Conference Proceedings 1990., Fifth Annual, March 1990, pp. 275-284.

[8] Yuancheng Ren, Ming Xu, Jinghai Zhou and F. C. Lee, "Analytical loss model of power MOSFET," in *IEEE Transactions on Power Electronics*, vol. 21, no. 2, pp. 310-319, March 2006.

[9] J. K. Murali, Chandrasekar V, Udaya Sagar V, S. Mohan, " Analysis, Estimation and Minimization of Power Loss in CCM Operated PSFB Converter," in *IEEE International Conference on Power Electronics, Drives and Energy Systems (PEDES)* 2016.

[10] E. Agheb, M. A. Bahmani, H. K. Høidalen, and T. Thiringer, "Core loss behavior in high frequency high power transformers—II: Arbitrary excitation," *Journal of Renewable and Sustainable Energy 4*, vol.4, Issue:3, pp: 033113 June 2011.